

NUMERICAL ANALYSIS OF PLASMA PROPERTIES IN THE
GLOW DISCHARGE: ACCURACY AND APPLICABILITY OF
SIMPLE AND EXTENDED FLUID MODELS

A THESIS SUBMITTED TO
THE GRADUATE SCHOOL OF NATURAL AND APPLIED SCIENCES
OF
MIDDLE EAST TECHNICAL UNIVERSITY

BY

KORAY KAYMAZLAR

IN PARTIAL FULFILLMENT OF THE REQUIREMENTS
FOR
THE DEGREE OF MASTER OF SCIENCE
IN
PHYSICS

JANUARY 2017

Approval of the thesis:

**NUMERICAL ANALYSIS OF PLASMA PROPERTIES IN THE
GLOW DISCHARGE: ACCURACY AND APPLICABILITY OF
SIMPLE AND EXTENDED FLUID MODELS**

submitted by **KORAY KAYMAZLAR** in partial fulfillment of the requirements for the degree of **Master of Science in Physics Department, Middle East Technical University** by,

Prof. Dr. Gülbin Dural Ünver
Dean, Graduate School of **Natural and Applied Sciences** _____

Prof. Dr. Sadi Turgut
Head of Department, **Physics** _____

Assoc. Prof. Dr. İsmail Rafatov
Supervisor, **Physics Department, METU** _____

Examining Committee Members:

Assoc. Prof. Dr. Serhat Çakır
Physics Department, METU _____

Assoc. Prof. Dr. İsmail Rafatov
Physics Department, METU _____

Assoc. Prof. Dr. Burak Yedierler
Physics Department, METU _____

Assoc. Prof. Dr. Hakan Altan
Physics Department, METU _____

Assist. Prof. Dr. Kemal Efe Eseller
Electrical and Electronics Eng. Dept., Atılım University _____

Date: _____

I hereby declare that all information in this document has been obtained and presented in accordance with academic rules and ethical conduct. I also declare that, as required by these rules and conduct, I have fully cited and referenced all material and results that are not original to this work.

Name, Last Name: KORAY KAYMAZLAR

Signature :

ABSTRACT

NUMERICAL ANALYSIS OF PLASMA PROPERTIES IN THE GLOW DISCHARGE: ACCURACY AND APPLICABILITY OF SIMPLE AND EXTENDED FLUID MODELS

KAYMAZLAR, KORAY

M.S., Department of Physics

Supervisor : Assoc. Prof. Dr. İsmail Rafatov

January 2017, 56 pages

The work deals with numerical investigation of physical processes in the gas discharge plasma. Numerical models are based on the fluid description of plasma, with drift-diffusion approximation for charged particle fluxes. First, we developed a “simple” fluid model, consisted of continuity equations for electrons and ions, coupled to Poisson equation for electric field. Next, we extended this model by incorporating the electron Boltzmann equation module, such that the electron transport parameters (mobility and diffusion) as well as the rates of electron induced plasma-chemical reactions are determined as functions of the local electric field, from convolution of the electron energy distribution function. The numerical method is based on the Method of Lines, where discretization in the coordinate space (as well as in the energy space for Boltzmann equation) is done by the Scharfetter-Gummel scheme. All numerical codes are developed using MATLAB package. Computational tests are carried out for glow discharge plasma in argon. Comparison of computed plasma parameters (such as the elec-

tron and ion densities, the electric field and potential, the current-voltage curves) obtained by “simple” and “extended” fluid models with one another and with experimental data allow to determine the accuracy and the ranges of applicability of these models.

Keywords: plasma, glow discharge, method of lines, fluid model

ÖZ

İŞİLTİLİ DEŞARJIN PLAZMA ÖZELLİKLERİNİN NUMERİK ANALİZİ: BASİT VE GENİŞLETİLMİŞ AKIŞKAN MODELLERİNİN DOĞRULUĞU VE UYGULANABİLİRLİĞİ

KAYMAZLAR, KORAY

Yüksek Lisans, Fizik Bölümü

Tez Yöneticisi : Doç. Dr. İsmail Rafatov

Ocak 2017 , 56 sayfa

Bu çalışma, ışıltılı deşarj plazmasındaki fiziksel süreçlerin nümerik analizi ile ilgilidir. Nümerik modeller, plazmanın akışkan tasviri için yüklü parçacıkların akılarının sürüklenme ve yayılım yaklaşımı üzerine kuruludur. İlk olarak, electron ve iyonların devamlılık denklemlerini dahil eden ve elektrik alan için Poisson denklemine bağlı bir "yalın" akışkan modeli oluşturuldu. Daha sonra, elektron Boltzmann denklemi için bir modül eklenmesi ile elektron enerji dağılımı fonksiyonu kullanılarak elektron taşıma parametreleri (hareketlilik ve yayılım) ve elektronların katıldığı plazma-kimyasal reaksiyon hızları yerel elektrik alanın fonksiyonu olarak hesaplanarak model genişletilmiştir. Nümerik yöntem ayrıklaştırmanın koordinat uzayında (Boltzmann denklemi çözümü için enerji uzayında) Scharfetter-Gummel şemasında yapıldığı çizgiler yöntemidir (Method of Lines). Nümerik kodlar MATLAB ortamında geliştirilmiştir. Hesaplama testleri argon ışıltılı deşarj plazma için yapılmıştır. "Yalın" ve "genişletilmiş" akışkan

modellerinden hesaplanmış plazma verilerinin (elektron ve iyon yođunlukları, elektrik alan, gerilim, akım-voltaj eđrisi gibi) birbirleri ve deneysel veriler ile karşılaştırılmaları dođruluk ve uygulanabilirlik bölgelerinin belirlenmesini mümkün kılmıştır.

Anahtar Kelimeler: plazma, ısıtılı deşarj, çizgiler metodu, akışkan modeli

dedicated to Assoc. Prof. Dr. Korkut Okan Ozansoy

ACKNOWLEDGMENTS

I am most thankful to my supervisor Assoc. Prof. Dr. İsmail Rafatov for his guidance during my study.

I am also thankful to Ender Eylenceoğlu for stimulating discussions and interpreting the results.

Finally, I would like to thank to my family for always encouraging me to finish my study and giving their support to my decisions in my life.

TABLE OF CONTENTS

ABSTRACT	v
ÖZ	vii
ACKNOWLEDGMENTS	x
TABLE OF CONTENTS	xi
LIST OF TABLES	xiii
LIST OF FIGURES	xiv
LIST OF ABBREVIATIONS	xviii
CHAPTERS	
1 INTRODUCTION	1
1.1 Classification of Plasmas	2
1.2 Glow Discharges	3
1.3 Plasma Modelling	4
1.4 Aims and Motivations	6
1.4.1 Organization of the Thesis	8
2 MODELS	9
2.1 Governing Equations	9
2.1.1 Two-Fluid Plasma Model	10

2.2	1D Simple and Extended Fluid Models	13
2.3	Parameter Regime	14
2.4	Boundary Conditions	15
3	NUMERICAL METHODS	17
3.1	Method of Lines	17
3.2	Finite Volume Method	18
3.2.1	Central Difference Scheme	20
3.2.2	Upwind Scheme	20
3.2.3	Exponential Scheme	22
3.2.4	Generalization of Formulation	23
4	BOLTZMANN EQUATION MODULE	25
4.1	Equations for BE Module	25
4.2	Results of BE Solver	29
5	RESULTS OF THE FLUID MODELLING	37
5.1	CVCs and Spatial Distributions	37
6	CONCLUSION	53
	REFERENCES	55

LIST OF TABLES

TABLES

Table 2.1	Parameters used in simple fluid (S.F.) and extended fluid (E.F.) models.	15
Table 3.1	The $A(P)$ function and corresponding discretization schemes.	23

LIST OF FIGURES

FIGURES

Figure 1.1 Adequate plasma models as functions of system size and pressure [13].	6
Figure 1.2 An example of CVC curve. Figure is adapted from [14].	7
Figure 1.3 A schematic of a DC discharge tube. Figure is adapted from [17].	7
Figure 2.1 A DC discharge system with external circuit. The figure is adapted from [22].	16
Figure 3.1 Control Volume in 1D.	18
Figure 4.1 Comparison of EEDFs obtained from BE solver and from BOLSIG+[28] for two different E/N values.	30
Figure 4.2 EEDFs obtained from BE solver for temporal and spatial growth at $E/N = 600Td$	31
Figure 4.3 EEDFs obtained from BE solver for various reduced E -fields.	32
Figure 4.4 EEDFs obtained from BE solver for various ionization degrees n_e/N_g at reduced electric field E/N value 10 Td.	32
Figure 4.5 Electron mobility μ_e curves obtained from BE solver and compared with that from Ref. [5].	33

Figure 4.6 Electron diffusion coefficient D_e obtained from BE solver and compared with that from Ref. [5].	33
Figure 4.7 Townsend coefficient α obtained from BE solver and compared with formula from Ref. [4].	34
Figure 4.8 Elastic collision frequency ν_{ie} obtained from BE solver and compared with that from Ref. [5].	35
Figure 4.9 Ionization rate coefficient k_{iz} obtained from BE solver and compared with that from Ref. [5].	35
Figure 4.10 Excitation rate coefficient obtained from BE solver and compared with Ref. [5].	36
Figure 5.1 CVC curves corresponding to simple fluid, extended fluid (LFA) with spatial and temporal growth, CVC curve from extended fluid (LMEA) model [5] and two plotted experimental data from [15] and [16]. Discharge is in argon and discharge gap is 1 cm	38
Figure 5.2 Spatial distributions of particle densities n_e and n_i obtained from the simple and extended fluid models in abnormal regime. Discharge is in argon gas, $p = 3$ Torr, $J = 45$ A/m ² and discharge gap is 1 cm.	39
Figure 5.3 Spatial distribution of ionization rates obtained from simple and extended fluid models in abnormal regime. Conditions are the same as in Fig. 5.2.	40
Figure 5.4 Spatial distribution of potential Φ obtained from the simple and extended fluid models in abnormal regime. Conditions are the same as in Fig. 5.2.	41
Figure 5.5 Spatial distribution of electric field E obtained from the simple and extended fluid models in abnormal regime. Conditions are the same as in Fig. 5.2.	41

Figure 5.6 Spatial distribution of ion, electron and total current densities J_i , J_e and J_t obtained from the simple and extended fluid models in abnormal regime. Conditions are the same as in Fig. 5.2.	42
Figure 5.7 Spatial distributions of particle densities n_e and n_i obtained from the simple and extended fluid models in normal regime. Discharge is in argon gas, $p = 3$ Torr, $J = 3 A/m^2$ and discharge gap is 1 cm.	43
Figure 5.8 Spatial distribution of ionization rates obtained from simple and extended fluid models in normal regime. Conditions are the same as in Fig. 5.7.	44
Figure 5.9 Spatial distribution of potential Φ obtained from the simple and extended fluid models in normal regime. Conditions are the same as in Fig. 5.7.	45
Figure 5.10 Spatial distribution of electric field E obtained from the simple and extended fluid models in normal regime. Conditions are the same as in Fig.5.7.	45
Figure 5.11 Spatial distribution of ion, electron and total current densities J_i , J_e and J_t obtained from the simple and extended fluid models in normal regime. Conditions are the same as in Fig. 5.7.	46
Figure 5.12 Spatial distributions of particle densities n_e and n_i obtained from the simple and extended fluid models in subnormal regime. Discharge is in argon gas, $p = 3$ Torr, $J = 0.19 A/m^2$ and discharge gap is 1 cm.	47
Figure 5.13 Spatial distribution of ionization rates obtained from the simple and extended fluid models in subnormal regime. Conditions are the same as in Fig. 5.12.	48
Figure 5.14 Spatial distribution of potential Φ obtained from the simple and extended fluid models in subnormal regime. Conditions are the same as in Fig. 5.12.	49

Figure 5.15 Spatial distribution of electric field E obtained from the simple and extended fluid models in subnormal regime. Conditions are the same as in Fig. 5.12. 49

Figure 5.16 Spatial distribution of ion, electron and total current densities J_i , J_e and J_t obtained from the simple and extended fluid models in subnormal regime. Conditions are the same as in Fig. 5.12. 50

LIST OF ABBREVIATIONS

DC	Direct Current
MOL	Method of Lines
PDE	Partial Differential Equation
ODE	Ordinary Differential Equation
FVM	Finite Volume Method
CV	Control Volume
LFA	Local Field Approximation
LMEA	Local Mean Energy Approximation
BE	Boltzman Equation
EEDF	Electron Energy Distribution Function
CVC	Current Voltage Characteristics

CHAPTER 1

INTRODUCTION

The word “plasma” means something molded in Greek [1]. The term “plasma” first used in 1929 by Irving Langmuir (1881 - 1957) to define the jelly like behavior of ionized gas. Later, it was generally accepted that the plasma is the fourth state of the matter. In literature, plasma is usually defined as quasi-neutral substances that consists of free electrons, ionized atoms or ionized molecules and neutral species that display collective behavior due to Coulomb forces [2]. Quasi-neutrality means that the substance has locally almost the same number of electrons and ions.

The majority of the matter of the “observable” universe is in plasma state. Stars, nebulae, supernovas and lightning are examples of plasma that exist naturally. Fluorescent lights, noble gas lamps, fusion reactors and plasma TVs are applications where man made plasma is generated.

One way to form plasma is to heat gases to high temperatures. Thermal collisions cause ionization of the substance. Another way to generate plasma is applying electric field high enough to ionize the gas. Because of their small masses, electrons are easily accelerated and gain enough energy to ionize gas atoms. Plasmas generated by applied electric field are called gas discharges [3]. Energetic photons can cause to ionization if they collides gas atoms or molecules. This is called photoionization. Ionosphere is a good example for plasmas produced with photoionization.

1.1 Classification of Plasmas

Plasmas can be classified according to diverse features.

Temperature:

- Low temperature plasmas ($T_e < 100\text{eV}$)
- High temperature plasmas ($T_e > 100\text{eV}$)

Here T_e is the electron temperature.

Pressure:

- Low pressure plasmas ($p < 10$ Torr)
- Moderate pressure plasmas ($p = 10 - 100$ Torr)
- High pressure plasmas ($p > 100$ Torr)

Thermodynamic equilibrium:

- Non thermal or non equilibrium plasmas ($T_e \gg T_i$)
- Thermal or equilibrium plasmas ($T_e \sim T_i$)

Here T_i is the ion temperature.

Ionization degree:

- Weakly ionized plasmas (below 10^{-3})
- Fully ionized plasmas (close to 1)

Frequency of applied voltage:

- DC discharge plasmas
- Pulsed DC discharge plasmas (kHz)
- RF discharge plasmas (MHz)

- Microwave discharge plasmas (GHz)
- Optical (laser sustained) plasmas

1.2 Glow Discharges

The main subject of the gas discharge physics is to study the current flow through the ionized gas and ionization of gas by the applied electric field [4]. Gas discharges can be sustained by applied voltage between two electrodes of a discharge tube containing ionized gas at adequate pressure. Initially, the tube is filled with an inert gas. At this stage the ionization is due to thermal collisions or cosmic radiation and its degree is very low.

Applied field accelerates free electrons and ions. These free charge carriers with sufficiently high energy, make collisions with the neutral atoms. These collisions result in excitation ($e + Ar \rightarrow e + Ar^*$) or ionization ($e + Ar \rightarrow 2e + Ar^+$) of the atoms. Bounded electrons jump up to higher energy states due to the excitations. When these electrons fall back lower energy states, they emit a characteristic radiation. This process is responsible for the glow in the discharge. Ionization occurs when free charge carriers have enough energy to ionize neutral species. The accelerated ions directed towards the cathode and hitting it cause secondary electron emission [5]. Depending on the amplitude of the applied voltage, a non self-sustained or self-sustained plasma may develop.

The importance of glow discharges comes from their industrial applications [6]. Light emitting property of gas discharge plasmas is exploited in light industry and display technology [7]. Fluorescent lamps are the most familiar examples of the applications of gas discharges. Colorful advertisements in streets are nothing but glow discharges sustained in an inert gas like neon. It is now becoming less popular but, plasma TVs are also good example for usage of gas discharges in display technology. Gas lasers can also take place in this category. One of the most important application is in microelectronic industry. Gas discharge plasmas are employed in many steps for microfabrication of ICs. Prominent examples are gas discharges for sputtering metals on superconducting films, growing oxide films on semiconductors and plasma-enhanced chemical vapor depositions. Gas dis-

charges are also used in microelectronic fabrication for implantation of dopant atoms and removing films like photoresists or polymer films. Furthermore, gas discharge plasmas have applications in analytical chemistry, environmental applications and material processing like coating [7].

1.3 Plasma Modelling

Importance of studies of gas discharge is due to applications in both industry and science. In order to able to design and optimize the plasma systems, a deep understanding of processes in gas discharges is required. Experiments on plasma and numerical modelling of plasma are the ways to gain such an understanding. However, experimental studies can be costly and time consuming. Moreover, given the space and the time scales of the measurements can be extremely complicated or even impossible. Analytical solutions are available in exceptional situations for idealized models. However, assumptions for idealized models are valid for narrow limited ranges and they are not suitable for most of the cases [8]. Therefore, in general, numerical studies allow to analyse and predict plasma properties of such systems. Commonly used plasma models are classified into kinetic/kinetic-particle models, fluid models and hybrid models.

A plasma medium like a discharge tube has too many particles to consider them individually even for advanced computers. Kinetic model considers particle ensembles instead of treating them individually via statistical tools [8],[9]. Distribution function $f(\mathbf{r}, \mathbf{v}, t)$ is defined in a 7D phase space. Evolution of the distribution function is governed by the Boltzmann equation. Solving Boltzmann equation in 7D is not an easy task. Conventionally, distribution function is decomposed before solving the Boltzmann equation [10]. Commonly used two-term approximation is a good example for this approach. Particle method (particle in cell method, PIC) which sometimes is classified as kinetic-particle model, keep tracks an ensemble of particles individually according to fundamental laws (Newton, Lorents, Maxwell). PIC simulations are better for representing collisional processes [11]. PIC method is best suited for low pressure systems with simple chemistry in which the number of particle species is small [8].

Fluid model is derived taking velocity moments of Boltzmann equation. These moments (0^{th} , 1^{st} and 2^{nd}) produce set of equations which are mass, momentum and energy conservation equations. Solution of the fluid equations lead to the macroscopic quantities like particle densities and fluid velocities. Fluid model is usually suitable for discharges at relatively high pressure [11]. Further simplifications of fluid model lead to the drift-diffusion approximation, which is very common in models of gas discharges. In the drift-diffusion models with the local field approximation (LFA), the transport and reaction rate coefficients are determined as functions of local electric field. Another approximation alternative to LFA is local mean energy approximation (LMEA), in which transport and reaction rate coefficients are functions of local mean energy. The main advantage of the fluid model compared to kinetic model is that it requires less computational work.

Hybrid model is the combination of fluid and kinetic-particle model. In this model, ions and less energetic (slow) electrons are described by fluid equations. For energetic (fast) electrons Monte-Carlo (MC) simulation is employed [12]. MC technique can be also applied for calculation of transport and reaction rate coefficients for fluid equations [8].

Following Fig. 1.1 relates the pressure and the scale of the plasma system with the appropriate theoretical description.

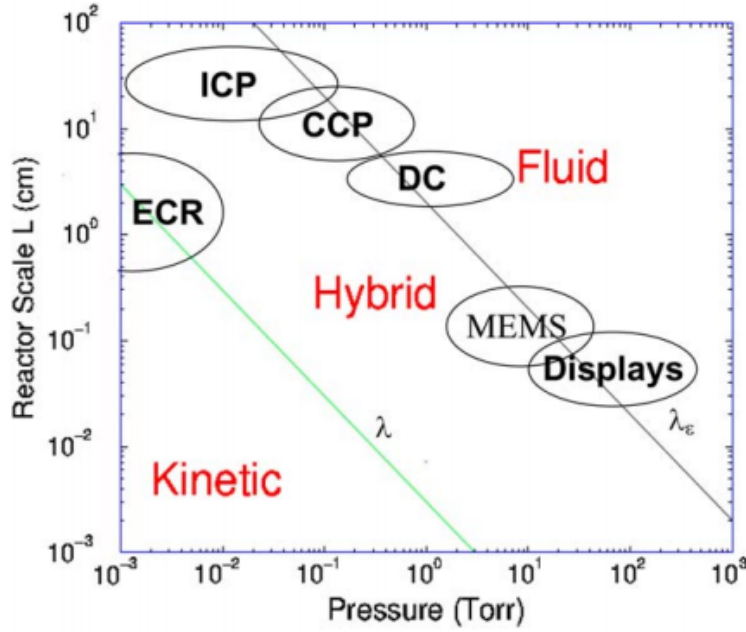


Figure 1.1: Adequate plasma models as functions of system size and pressure [13].

1.4 Aims and Motivations

One of the most important characteristics of the glow discharge is the current-voltage (CVC) curve. It indicates the current through the tube and the corresponding anode voltage. There are three different regimes which are subjects of this study in the glow regions of the CVC curve, as it is illustrated in Fig. 1.2. These regimes are named abnormal, normal and subnormal regimes. The system express different characteristics in these regimes.

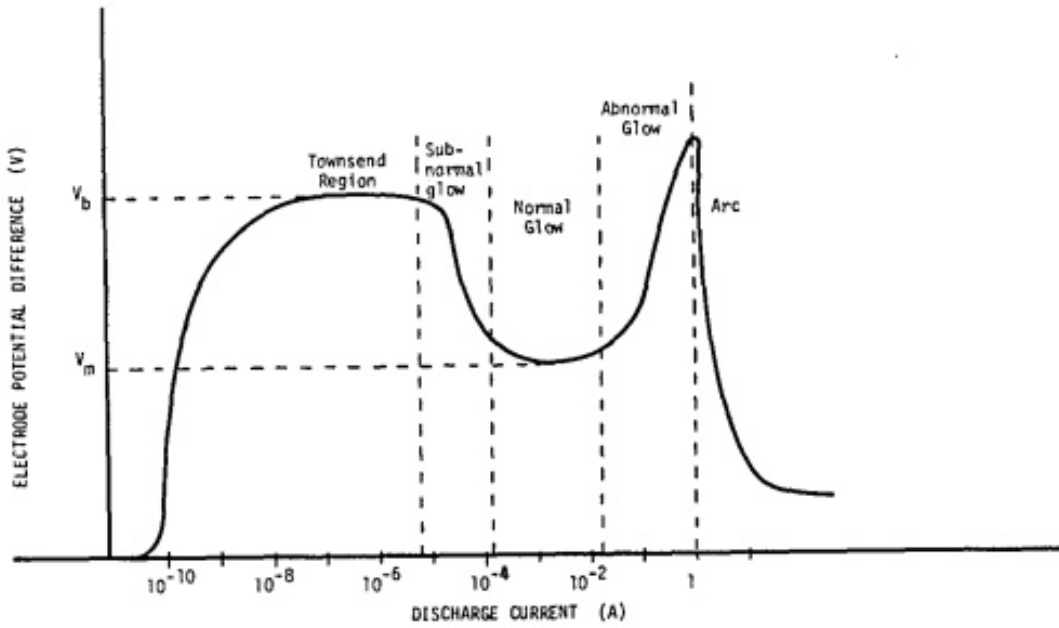


Figure 1.2: An example of CVC curve. Figure is adapted from [14].

A plasma column can be described by spatial distribution of its parameters, which are the densities of species, voltage, electric field, etc.

The aim of this thesis is the numerical investigation of physical processes in the DC gas discharge plasma. Results of our models which are based on fluid description of plasma with drift-diffusion approximation are compared with the results obtained in the previous works (e.g. [5],[15] and [16]). Comparisons are based on CVC curves and spatial distributions of plasma parameters in the abnormal, normal and subnormal regimes.

Numerical calculations are done for a DC glow discharge tube containing argon gas under conditions similar with the Refs. [5], [15] and [16].

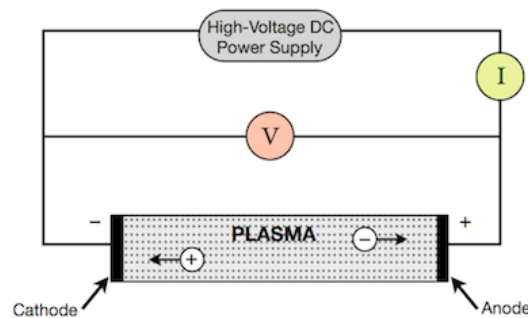


Figure 1.3: A schematic of a DC discharge tube. Figure is adapted from [17].

Models we derived are simple and extended fluid models based on two fluid plasma model with drift-diffusion approximation for particle fluxes. Numerical technique is MOL (Method of Lines), where the spatial discretization is done by the FVM (Finite Volume Method).

1.4.1 Organization of the Thesis

In Chapter 2, the derivation of two-fluid model of plasma from Boltzmann equations is explained. Subsequently, simple and extended fluid models of plasma are introduced. Chapter 3 describes the numerical methods, where the MOL technique and discretization schemes by FVM are presented. In Chapter 4, we introduce Boltzmann equation (BE) solver module for deriving the transport parameters and reaction rates. Then, results obtained from the solver are compared with parameters used in [5]. In Chapter 5, CVC curves obtained from numerical calculations are presented and compared with those from [5],[15] and [16]. Later, spatial distributions of plasma parameters calculated in abnormal, normal and subnormal regimes of DC discharges are presented and compared with [5]. In Chapter 6 the conclusions are presented.

CHAPTER 2

MODELS

A discharge volume contains a great number of charged particles of the order 10^{16} at pressure $p = 1$ Torr. Keeping track of parameters like position and velocity of these particles one by one is impossible even for supercomputers. Therefore, it is not practical to consider behavior of the particles individually. For this reason fluid model of plasma has been developed. Derivation of fluid model is based on the kinetic model of plasma which uses statistical tools for dynamical behavior of plasma [18]. Further, the fluid model is reduced to the drift-diffusion models for plasma.

2.1 Governing Equations

Kinetic Boltzmann equation for one species of particles can be written as

$$\frac{\partial f}{\partial t} + \nabla_r \cdot \mathbf{u}f + \frac{q}{m} \nabla_u \cdot (\mathbf{E} + \mathbf{u} \times \mathbf{B})f = \frac{\delta f}{\delta t} \Big|_{coll},$$

where m is the mass of the particle, q is the charge, \mathbf{E} is the electric field and \mathbf{B} is the magnetic field. Number of the particles in phase space volume element is

$$f(\mathbf{r}, \mathbf{u}, t) d\mathbf{r} d\mathbf{u},$$

where \mathbf{r} and \mathbf{u} are vectors in the position and velocity spaces respectively. Additionally, Maxwell's equations are also needed to be supplied to kinetic model. The fluid equations can be derived from the Boltzmann equation by taking its zeroth, first and second moments [19].

0th moment produces the continuity equation

$$\frac{\partial n}{\partial t} + \nabla \cdot (\mathbf{v}n) = 0.$$

1st moment produces the momentum equation

$$mn \frac{d\mathbf{v}}{dt} = qn(\mathbf{E} + \mathbf{v} \times \mathbf{B}) - \nabla p + \boldsymbol{\nu}.$$

2nd moment gives the energy equation

$$\frac{3}{2}n \frac{dk_B T}{dt} + p \nabla \cdot \mathbf{v} = 0.$$

In these equations p is the pressure, T is the temperature, k_B is the Boltzmann constant, n represents the particle density and \mathbf{v} is the fluid velocity, which are calculated as

$$n(\mathbf{r}, t) = \int f(\mathbf{r}, \mathbf{u}, t) d\mathbf{u},$$

$$\mathbf{v}(\mathbf{r}, t) = \frac{1}{n} \int \mathbf{u} f(\mathbf{r}, \mathbf{u}, t) d\mathbf{u}.$$

2.1.1 Two-Fluid Plasma Model

Two fluid plasma model is constructed using fluid equations described above. It is called two-fluid since it considers fluids of electron and ion separately. According to this definition, equations can be written for electrons and ions as follows:

$$\frac{\partial n_e}{\partial t} + \nabla \cdot (\mathbf{v}_e n_e) = S_e, \quad (2.1)$$

$$m_e n_e \frac{d\mathbf{v}_e}{dt} = q_e n_e (\mathbf{E} + \mathbf{v}_e \times \mathbf{B}) - \nabla p_e + \mathbf{f}_{ei}, \quad (2.2)$$

$$\frac{3}{2} n_e \frac{dk_B T_e}{dt} + p_e \nabla \cdot \mathbf{v}_e = Q_{ei}, \quad (2.3)$$

$$\frac{\partial n_i}{\partial t} + \nabla \cdot (\mathbf{v}_i n_i) = S_i, \quad (2.4)$$

$$m_i n_i \frac{d\mathbf{v}_i}{dt} = q_i n_i (\mathbf{E} + \mathbf{v}_i \times \mathbf{B}) - \nabla p_i + \mathbf{f}_{ie} \quad (2.5)$$

$$\frac{3}{2} n_i \frac{dk_B T_i}{dt} + p_i \nabla \cdot \mathbf{v}_i = Q_{ie}. \quad (2.6)$$

These equations are also needed to be supplied by the Maxwell's equations to have a self consisted model:

$$\nabla \times \mathbf{B} = \mu_0 \mathbf{J} + \frac{1}{c^2} \frac{\partial \mathbf{E}}{\partial t}, \quad (2.7)$$

$$\nabla \cdot \mathbf{B} = 0, \quad (2.8)$$

$$\nabla \times \mathbf{E} = -\frac{\partial \mathbf{B}}{\partial t}, \quad (2.9)$$

$$\nabla \cdot \mathbf{E} = \frac{\sigma}{\epsilon_0}. \quad (2.10)$$

In these equations n_e and n_i represent the densities of electrons and ions, S_e and S_i represents the source terms which represents creation or vanishing of the charged particles, m_e and m_i are masses of the particles, p_e and p_i are the pressures, \mathbf{E} is the electric field and \mathbf{B} is the magnetic flux density, k_B is the Boltzmann constant, ϵ_0 is the permittivity of vacuum. Moreover, σ and \mathbf{J} represent the charge and the current densities:

$$\sigma = n_i q_i + n_e q_e,$$

$$\mathbf{J} = n_i q_i \mathbf{v}_i + n_e q_e \mathbf{v}_e.$$

The momentum lost per collision is related to the relative velocity

$$\mathbf{f}_{e,i} = -\nu_{ei} m_e n_e (\mathbf{v}_e - \mathbf{v}_i),$$

where $\nu_{e,i}$ is the electron-ion collision frequency [19].

Momentum conservation equations (2.2) and (2.5) can be written as

$$\begin{aligned} & \rho_e \frac{\partial \mathbf{v}_e}{\partial t} + \rho_e (\mathbf{v}_e \cdot \nabla) \mathbf{v}_e = \\ & -\nabla p_e - en_e (\mathbf{E} + \mathbf{v}_e \times \mathbf{B}) - \nu_{en} m_e n_e (\mathbf{v}_e - \mathbf{v}_n) - \nu_{ei} m_e n_e (\mathbf{v}_e - \mathbf{v}_i) \end{aligned}$$

and

$$\begin{aligned} & \rho_i \frac{\partial \mathbf{v}_i}{\partial t} + \rho_i (\mathbf{v}_i \cdot \nabla) \mathbf{v}_i = \\ & -\nabla p_i + en_i (\mathbf{E} + \mathbf{v}_i \times \mathbf{B}) - \nu_{ie} m_i n_i (\mathbf{v}_i - \mathbf{v}_e) - \nu_{in} m_e n_e (\mathbf{v}_i - \mathbf{v}_n), \end{aligned}$$

where \mathbf{v}_n is velocity of neutral gas atoms. Considering $m_e \ll m_i$, it gives

$$\rho_e (\mathbf{v}_e \cdot \nabla) \mathbf{v}_e \ll \rho_i (\mathbf{v}_i \cdot \nabla) \mathbf{v}_i.$$

Then the momentum equations can be simplified:

$$-\nabla p_e - en_e (\mathbf{E} + \mathbf{v}_e \times \mathbf{B}) - \nu_{en} m_e n_e (\mathbf{v}_e - \mathbf{v}_n) - \nu_{ei} m_e n_e (\mathbf{v}_e - \mathbf{v}_i) = 0.$$

For $\mathbf{v}_e \gg \mathbf{v}_n, \mathbf{v}_i$ and $p_e = n_e k_B T_e$, simplification proceeds to

$$k_B T_e \nabla n_e + e n_e \mathbf{E} + e n_e (\mathbf{v}_e \times \mathbf{B}) + (m_e \nu_e) n_e \mathbf{v}_e = 0.$$

It can be written as

$$n_e \mathbf{v}_e = -D_e \nabla n_e - \mu_e n_e \mathbf{E} - \mu_e n_e (\mathbf{v}_e \times \mathbf{B}), \quad (2.11)$$

where the mobility of the electrons is

$$\mu_e \equiv \frac{e}{m_e \nu_e}$$

and the electron diffusion coefficient is

$$D_e \equiv \frac{k_B T_e}{e} \mu_e.$$

Here the averaged electron collision frequency is taken approximately as $\nu_e = \nu_{en} + \nu_{ei}$.

In a similar way,

$$-\nabla p_i + e n_i (\mathbf{E} + \mathbf{v}_i \times \mathbf{B}) - \nu_{ie} m_i n_i (\mathbf{v}_i - \mathbf{v}_e) - \nu_{in} m_i n_i (\mathbf{v}_i - \mathbf{v}_n) = 0.$$

Assuming

$$\nu_{ie} m_i n_i (\mathbf{v}_i - \mathbf{v}_e) = -\nu_{ei} m_e n_e (\mathbf{v}_e - \mathbf{v}_i),$$

$$\mathbf{v}_n = 0,$$

and $m_e \nu_e \ll m_i \nu_{in}$, we get

$$n_i \mathbf{v}_i = -D_i \nabla n_i + \mu_i n_i \mathbf{E} + \mu_i n_i (\mathbf{v}_i \times \mathbf{B}), \quad (2.12)$$

where the mobility of the ions is defined as

$$\mu_i \equiv \frac{e}{m_i \nu_i}$$

and the ion diffusion coefficient is [20, 21]

$$D_i \equiv \frac{k_B T_i}{e} \mu_i$$

Putting the results above into the continuity equations (2.1) and (2.4) and neglecting magnetic field \mathbf{B} leads to the two fluid equations with drift-diffusion approximation:

$$\frac{\partial n_e}{\partial t} + \nabla \cdot (-\mu_e n_e \mathbf{E} - D_e \nabla n_e) = S_e, \quad (2.13)$$

$$\frac{\partial n_i}{\partial t} + \nabla \cdot (\mu_i n_i \mathbf{E} - D_i \nabla n_i) = S_i. \quad (2.14)$$

Two processes, ionization and recombination, determine the source terms, for example,

$$S_e = S_i = \alpha(E, p)|\mathbf{\Gamma}_e| - \beta n_i n_e,$$

where α is the Townsend ionization coefficient and β is the recombination coefficient and

$$\mathbf{\Gamma}_e = -\mu_e n_e \mathbf{E} - D_e \nabla n_e$$

is the total electron flux density. The set of equations is completed with the Poisson equation for electric potential

$$-\nabla^2 \Phi = \frac{e}{\epsilon_0} (n_i - n_e).$$

Finally, the strength of the electric field is calculated from the relation

$$\mathbf{E} = -\nabla \Phi.$$

In this work, α , β and γ processes are considered. α process is the ionization through collision of electrons with neutral atoms. β process is the recombination process where electrons and ions combine and become neutral atoms. γ process is secondary emission where ions hit the cathode and cause emission of electrons.

2.2 1D Simple and Extended Fluid Models

In this study, 1D simple and extended fluid models are constructed and investigated. Simple fluid model is examined first and validation of numerical model is carried out.

In simple fluid models transport parameters like mobility μ_e and μ_i , diffusion coefficients D_e and D_i are usually defined as constants. In more detailed models like extended fluid models, local field approximation (LFA) is a way to determine transport and reaction rate coefficients. In this case transport and reaction rate coefficients are calculated from the solution of kinetic Boltzmann equation as functions of the reduced electric field E/N .

Extended fluid model with local mean energy approximation (LMEA) offers another alternative to calculate the transport coefficients by solving the kinetic Boltzmann equation again for the value of reduced electric field E/N which corresponds the value of electron mean energy, $\bar{\epsilon}$ at that point. This approach comes

with a price that energy balance equation is needed to add into set of equations [22]. A computational module can be generated to solve kinetic Boltzmann equation and derive transport and reaction coefficients as functions of reduced electric field E/N . However, it is time consuming to use the module for each node on the grid. In this work, the coefficients are interpolated from the look-up tables that were produced for a range of values of reduced electric field. Therefore, in this way, energy balance equation is excluded from the consideration and the calculations are simplified.

For 1D simple and extended fluid models with LFA the set of equations has the form

$$\frac{\partial n_e}{\partial t} - \frac{\partial}{\partial x} \left(\mu_e E n_e + D_e \frac{\partial n_e}{\partial x} \right) = S_e, \quad (2.15)$$

$$\frac{\partial n_e}{\partial t} - \frac{\partial}{\partial x} \left(-\mu_i E n_i + D_i \frac{\partial n_i}{\partial x} \right) = S_i, \quad (2.16)$$

$$\frac{\partial^2 \Phi}{\partial x^2} = -\frac{e}{\epsilon_0} (n_i - n_e). \quad (2.17)$$

The extended fluid model with LMEA includes additionally the energy equation for electrons [22]

$$\frac{\partial n_e}{\partial t} + \frac{\partial \Gamma_e}{\partial x} = -e \Gamma_e \cdot \mathbf{E} - \frac{3 m_e}{2 m_g} \nu_e n_e k_B (T_e - T_g) - \sum_j \Delta E_j R_j,$$

where

$$\begin{aligned} \Gamma_e &= -D_e \nabla n_e - \mu_e \mathbf{E} n_e, \\ n_e &= n_e \bar{\epsilon} \end{aligned}$$

and D_e , μ_e , ΔE_j , R_j and m_g are defined as in [22].

2.3 Parameter Regime

In this section parameters that are used in calculations are described. Numerical test are carried out for the DC glow discharge in argon. In the following table values of constant parameters for argon gas are listed. In case if a parameter is not a constant, the variable that they depend on is showed in parenthesis. Note that the gas density is obtained using the $N_g = p N_0$ relation. A and

B constants for argon gas are taken from the Yuri P. Raizer's book [4] and Townsend coefficient in the case of simple fluid model is calculated as

$$A p e^{-\frac{Bp}{|E|}}. \quad (2.18)$$

Symbol	Value(S.F.)	Value(LFA)	Unit	Definition
L	0.01	0.01	m	length of the tube
U	500	500	V	electric potential
R	10k - 10 M	10k - 10 M	Ω	resistance
C	1	1	pF	capacitance
p	3	3	$Torr$	pressure
μ_e	10	$\mu_e(E/N)$	$m^2/(sV)$	electron mobility
μ_i	0.08	0.08	$m^2/(sV)$	ion mobility
D_e	10	$D_e(E/N)$	m^2/s	electron diffusion coefficient
D_i	0.002	0.002	m^2/s	ion diffusion coefficient
α	$\alpha(A, B, E)$	$\alpha(E/N)$	m^{-1}	Townsend coefficient
A	1200	-	$m^2/Torr$	constant for T. coefficient
B	18000	-	$m^2/Torr$	constant for T. coefficient
β	2×10^{-13}	2×10^{-13}	m^3/s	recombination coefficient
γ	0.06	0.06	-	secondary emission coefficient
N_0	3.54×10^{22}	3.54×10^{22}	$m^{-3}/Torr$	gas density for 1 $Torr$
r	0.015	0.015	m	cathode radius
T_e	1	$T_e(E/N)$	eV	electron temperature
$T_g = T_i$	0.025	0.025	eV	ion or gas temperature

Table2.1: Parameters used in simple fluid (S.F.) and extended fluid (E.F.) models.

2.4 Boundary Conditions

The same boundary conditions as in [5] are applied for n_e and n_i in the models. These are defined as directed fluxes

$$\hat{\mathbf{n}} \cdot \mathbf{\Gamma}_e = \frac{1}{4} n_e v_e - \omega_e \mu_e n_e (\hat{\mathbf{n}} \cdot \mathbf{E}) - \kappa \gamma \hat{\mathbf{n}} \cdot \mathbf{\Gamma}_i, \quad (2.19)$$

$$\hat{\mathbf{n}} \cdot \mathbf{\Gamma}_i = \frac{1}{4} n_i v_i + \omega_i \mu_i n_i (\hat{\mathbf{n}} \cdot \mathbf{E}), \quad (2.20)$$

where $\hat{\mathbf{n}}$ is the unit vector directed towards the cathode and $\omega_{e,i} = 1$ when fluxes are directed to the walls and 0 otherwise. Moreover, $\kappa = 1$ at the cathode only and

$$v_{e,i} = \sqrt{\frac{8\pi T_{e,i}}{em_{e,i}}}$$

are particle thermal speeds.

Boundary conditions for potential at anode $\Phi = U_d$ is determined from the external circuit equation (see Fig.(2.1)):

$$\frac{dU_d}{dt} - \frac{1}{C} \left(I_d - \frac{U - U_d}{R} \right) = 0, \quad (2.21)$$

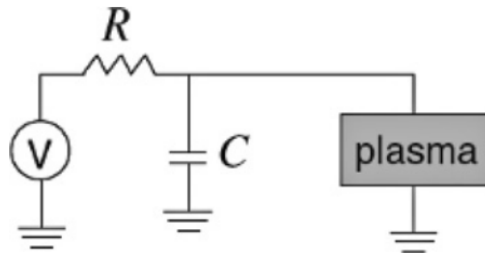


Figure 2.1: A DC discharge system with external circuit. The figure is adapted from [22].

where U_d is the anode voltage, C is the capacitance, I_d is the discharge current and R is the resistance, whose magnitudes are given in table 2.1. Since cathode side is grounded the boundary condition for that node is taken $\Phi = 0$.

CHAPTER 3

NUMERICAL METHODS

3.1 Method of Lines

Method of lines (MOL) is applied in this work to solve time-dependent partial differential equations (PDEs) [23]. This method is based on disintegration of PDE to N number of ordinary differential equations (ODEs). Here N is the number of nodes in the spatial grid for the PDE:

$$\text{PDE (having a grid of } N \text{ nodes)} \rightarrow N \times \text{ODEs}$$

After this disintegration the PDE problem is reduced to N number of initial value problems described by first order ODEs, where the values of the dependent variables at the spatial nodes at the initial time are the initial values of the corresponding ODEs. Solving the systems of ODEs individually and bringing together of the solution gives the solution of the PDE.

ODEs can be solved by generating a numerical code or using built in ODE solvers. In this work the MATLAB ODE solver ode15s was used. The command in the numerical code where ODE15s is used as follows:

```
options=odeset('Mass',M,'RelTol',reitol,'AbsTol',abstol);  
[t,u]=ode15s(pdefunc,timespan,IC,options);
```

The first line is for the basic setting options for the solver. AbsTol and RelTol set the solver desired tolerances of the computation. Mass represents the mass

matrix which allows the solver to distinguish between the ODE and DAE and apply an appropriate method. For example, for a space divided by N grid points, there are $3N$ ODE equations for electrons, ions and potential in the drift-diffusion model. Poisson equation for potential is time independent except for the anode node. Therefore, other than anode node the diagonal entries in Mass matrix for potential are set to be 0. Since the anode node is time dependent, the diagonal entry in Mass matrix for anode node is set to be 1. Therefore, when solving Poisson equation, ODE solver acts as a DAE solver for nodes other than the anode node.

The second command is the part of the code, where the algorithm sets where to save the results, the initial conditions, when to save the results and RHS (Right Hand Side) of the equations. The RHS of the equations is determined from FVM (Finite Volume Methods) methods as in the following section.

3.2 Finite Volume Method

As discussed above MOL creates a number of 1^{st} order ODEs to solve the PDE. The right hand side of these ODEs are determined by the discretization method in spatial domain. In this study, Finite Volume Method (FVM) is used. This method focuses to a small volume which is called the control volume (CV) in the spatial domain and considers the center of this volume and the fluxes through the walls of this volume element.

Here, P is the central point, W and E are left ("west") and right ("east")

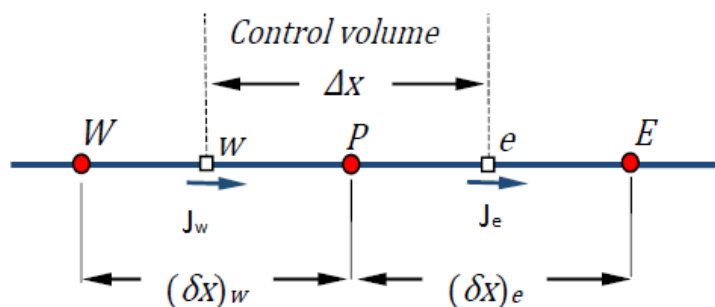


Figure 3.1: Control Volume in 1D.

nodes accordingly, w and e are the middle points between the nodes.

Consider the fluid equation with drift-diffusion approximation

$$\frac{\partial n_k}{\partial t} + \nabla \cdot (s_k \mu_k n_k E - D_k \nabla n_k) = S_k, \quad (3.1)$$

where k represents the species and can be omitted. Equation (3.1) can be written as

$$\frac{\partial n}{\partial t} + \frac{\partial J}{\partial x} = S, \quad (3.2)$$

where the total flux J is

$$J = s\mu En - D \frac{\partial n}{\partial x}. \quad (3.3)$$

If Eq. (3.2) is integrated over x in control volume, we have [24]

$$\frac{\partial}{\partial t} \int_{x_w}^{x_e} n dx + \int_{x_w}^{x_e} \frac{\partial J}{\partial x} dx = \int_{x_w}^{x_e} S dx.$$

It is assumed that S is constant in CV, so that

$$\frac{\partial n}{\partial t} \Delta x + (J_e - J_w) = S_p \Delta x$$

or

$$\frac{\partial n}{\partial t} = \frac{(J_w - J_e)}{\Delta x} + S_p \quad (3.4)$$

Looking at J_e closer,

$$J_e = \left(s\mu En - D \frac{\partial n}{\partial x} \right) \Big|_e = (s\mu En)|_e - D_e \frac{n_E - n_P}{(\delta_x)|_e}.$$

Using the notations

$$f_e = (s\mu E)|_e,$$

$$\Gamma_e = \left(\frac{D}{\delta_x} \right) \Big|_e,$$

we obtain

$$J_e = f_e n_e - \Gamma_e (n_E - n_P). \quad (3.5)$$

Similarly

$$J_w = f_w n_w - \Gamma_w (n_P - n_W).$$

Notice that Γ_e and Γ_w are always positive. The differential scheme takes the final form according to the definitions for n_e and n_w .

3.2.1 Central Difference Scheme

In central difference scheme, n_e is taken as follows:

$$n_e = 0.5(n_E + n_P).$$

Putting it into the equation (3.4), we have

$$\begin{aligned} J_e &= 0.5(n_E + n_P)f_e - \Gamma_e(n_E - n_P) \\ &= n_E(0.5f_e - \Gamma_e) + n_P(0.5f_e + \Gamma_e). \end{aligned}$$

Similarly,

$$n_w = 0.5(n_P + n_W)$$

and

$$J_w = n_W(0.5f_w + \Gamma_w) + n_P(0.5f_w - \Gamma_w).$$

Considering the term $J_w - J_e$, we have

$$\begin{aligned} J_w - J_e &= n_W(0.5f_w + \Gamma_w) + n_P(0.5f_w - \Gamma_w) - n_E(0.5f_e - \Gamma_e) - n_P(0.5f_e + \Gamma_e) \\ &= a_E n_E + a_W n_W - a_P n_P, \end{aligned} \tag{3.6}$$

where

$$\begin{aligned} a_E &= \Gamma_e - 0.5f_e, \\ a_W &= \Gamma_w + 0.5f_w, \\ a_P &= (\Gamma_e + 0.5f_e) + (\Gamma_w - 0.5f_w), \\ &= a_E + a_W + (f_e - f_w). \end{aligned}$$

3.2.2 Upwind Scheme

In upwind scheme, the value of n at the control volume walls are determined by direction of the flow (or the sign of the velocity). For our case the value at the "east" wall is

$$n_e = \begin{cases} n_P, & f_e > 0 \\ n_E, & f_e < 0 \end{cases}$$

Alternatively,

$$f_e n_e = n_P[|f_e, 0|] - n_E[|-f_e, 0|],$$

where $[| \cdot |]$ function returns the maximum element inside. Then,

$$\begin{aligned} J_e &= n_P[|f_e, 0|] - n_E[|-f_e, 0|] - \Gamma_e(n_E - n_P) \\ &= n_P(\Gamma_e + [|f_e, 0|]) - n_E(\Gamma_e + [|-f_e, 0|]) \\ &= n_P(\Gamma_e + [|f_e, 0|]) - a_E n_E, \end{aligned}$$

where

$$a_E = \Gamma_e + [|-f_e, 0|].$$

In a similar way,

$$n_w = \begin{cases} n_P, & f_w < 0 \\ n_W, & f_w > 0. \end{cases}$$

Alternatively

$$f_w n_w = -n_P[|-f_w, 0|] + n_W[|f_w, 0|],$$

and

$$\begin{aligned} J_w &= n_W[|f_w, 0|] - n_P[|-f_w, 0|] - \Gamma_w(n_P - n_W) \\ &= -n_P(\Gamma_w + [|-f_w, 0|]) + n_W(\Gamma_w + [|f_w, 0|]) \\ &= -n_P(\Gamma_w + [|-f_w, 0|]) + a_W n_W, \end{aligned}$$

where

$$a_W = \Gamma_w + [|f_w, 0|].$$

Again, $J_w - J_e$ term can be written as

$$\begin{aligned} J_w - J_e &= -n_P(\Gamma_w + [|-f_w, 0|]) + a_W n_W - n_P(\Gamma_e + [|-f_e, 0|]) + a_E n_E \\ &= a_E n_E + a_W n_W - a_P n_P, \end{aligned}$$

where

$$\begin{aligned} a_P &= \Gamma_w + [|-f_w, 0|] + \Gamma_e + [|f_e, 0|] \\ &= a_E + a_W + (f_e - f_w). \end{aligned}$$

Notice that formally this relation is similar to that obtained for the central difference scheme [24].

3.2.3 Exponential Scheme

Consider a steady situation

$$\frac{d}{dx}(s\mu En) = \frac{d}{dx}D \left(\frac{dn}{dx} \right)$$

in the domain $0 \leq x \leq L$ subject to boundary conditions

$$n|_{x=0} = n_0.$$

$$n|_{x=L} = n_L.$$

Its solution is

$$\frac{n - n_0}{n_L - n_0} = \frac{\exp(s\mu Ex/DL) - 1}{\exp(s\mu E/D) - 1}. \quad (3.7)$$

A parameter named Peclet number is define as

$$P \equiv \frac{s\mu E}{D/\delta_x} = \frac{f}{\Gamma}.$$

Then the equation (3.7) turns into

$$\frac{n - n_0}{n_L - n_0} = \frac{\exp(Px/L) - 1}{\exp(P) - 1}. \quad (3.8)$$

Putting Eq. (3.8) into Eq.(3.3) and substituting $n_0 = n_P$, $n_L = n_E$ and taking $\delta_x = L$ yields

$$J_e = f_e \left(n_P + \frac{n_p - n_E}{\exp(P_e) - 1} \right),$$

and similarly

$$J_w = f_w \left(n_W + \frac{n_W - n_P}{\exp(P_w) - 1} \right).$$

$J_w - J_e$ term can be written again in the form

$$J_w - J_e = a_E n_E + a_W n_W - a_P n_P,$$

where

$$\begin{aligned} a_E &= \frac{f_e}{\exp(P_e) - 1}, \\ a_W &= \frac{f_w \exp(P_w)}{\exp(P_w) - 1}, \\ a_P &= a_E + a_W + (f_e - f_w). \end{aligned}$$

In the literature [25], the exponential scheme is also called the Scharfetter - Gummel (S.G.) scheme.

3.2.4 Generalization of Formulation

Using the results above, Eq. (3.4) can be written as

$$\frac{\partial n}{\partial t} = \frac{a_E n_E + a_W n_W - a_P n_P}{\Delta x} + S_p. \quad (3.9)$$

A function depending on the Peclet number can be introduced to define any of these schemes. Definition of the functions $A(|P|)$ s and corresponding schemes are as in the table 3.1 [24]:

Scheme	$A(P)$
Central Difference	$1 - 0.5 P $
Upwind	1
Exponential (S.G.)	$ P /\exp(P)-1$

Table3.1: The $A(|P|)$ function and corresponding discretization schemes.

The terms in the equation (3.9) are also generalized according to the $A(|P|)$ function:

$$\begin{aligned} a_E &= \Gamma_e A(|P_e|) + [| - f_e, 0|], \\ a_W &= \Gamma_w A(|P_w|) + [| - f_e, 0|], \\ a_P &= a_E + a_W + (f_e - f_w). \end{aligned}$$

Thus, using these generalized equations, a numerical code can be designed, which will comprise all of these three schemes.

CHAPTER 4

BOLTZMANN EQUATION MODULE

As mentioned in chapter 2, extended fluid model for gas discharge employs the transport parameters and reaction rate coefficients, which are obtained from solution of Boltzmann equation (BE) for the electron energy distribution function (EEDF). For this purpose, BE module is developed to solve Boltzmann equation and calculate necessary parameters using two term approximation method as in [26].

4.1 Equations for BE Module

Consider Boltzmann equation for electrons in ionized gas:

$$\frac{\partial f}{\partial t} + \mathbf{v} \cdot \nabla f - \frac{e}{m} \mathbf{E} \cdot \nabla_v f = C[f]. \quad (4.1)$$

Here f is EEDF in seven dimensional phase space and C is the rate of change of it due to collisions. After assumptions of uniform electric field E and symmetric f in velocity space, BE in spherical coordinates is simplified to

$$\frac{\partial f}{\partial t} + v \cos \theta \frac{\partial f}{\partial z} - \frac{e}{m} E \left(\cos \theta \frac{\partial f}{\partial v} + \frac{\sin^2 \theta}{v} \frac{\partial f}{\partial \cos \theta} \right) = C[f]. \quad (4.2)$$

Here v is the magnitude of the velocity, z and θ are the the coordinates. Two term approximation simplifies the θ dependence. In two term approximation f is expanded in terms of Legendre polynomials and Eq. (4.2) is reconstructed accordingly for first the two terms of the expansion [26]. Results with higher accuracy can be obtained by taking for first six or more terms [27]. However,

first two terms already have useful results in most of the cases [26]. EEDF with two term approximation is written as

$$f(v, \cos \theta, z, t) = f_0(v, z, t) + f_1(v, z, t) \cos \theta, \quad (4.3)$$

where f is decomposed into isotropic velocity part f_0 and anisotropic velocity part f_1 [6]. Substituting Eq. (4.3) into (4.2) gives

$$\frac{\partial f_0}{\partial t} + \frac{\gamma}{3} \epsilon^{1/2} \frac{\partial f_1}{\partial z} - \frac{\gamma}{3} \epsilon^{-1/2} \frac{\partial}{\partial \epsilon} (\epsilon E f_1) = C_0, \quad (4.4)$$

$$\frac{\partial f_1}{\partial t} + \gamma \epsilon^{1/2} \frac{\partial f_0}{\partial z} - E \gamma \epsilon^{1/2} \frac{\partial f_0}{\partial \epsilon} = -N \sigma_m \gamma \epsilon^{1/2} f_1. \quad (4.5)$$

In these equations constant $\gamma = (2e/m)^{1/2}$, $\epsilon = (v/\gamma)^2$ is the electron energy, E is electric field and N is gas density, σ_m represents the total momentum cross-section

$$\sigma_m = \sum_k x_k \sigma_k, \quad (4.6)$$

where k indicates certain collision process, x_k is mole fraction, which is equal to one in this study. The term σ_k is effective momentum transfer cross-section for elastic collisions and total cross-section for inelastic collisions.

EEDF is separated as

$$f_0(\epsilon, z, t) = \frac{1}{2\pi\gamma^3} F_0(\epsilon) n(z, t), \quad (4.7)$$

$$f_1(\epsilon, z, t) = \frac{1}{2\pi\gamma^3} F_1(\epsilon) n(z, t). \quad (4.8)$$

Note that $F_{0,1}$ has only energy dependence and satisfy the following normalization condition

$$\int_0^\infty \epsilon^{1/2} F_0 d\epsilon = 1.$$

There are different ways to consider the growth of electron density. It is convenient to use exponential temporal growth without space dependence for analyzing pulsed Townsend experiments [26]. For this case, the rate of electron density growth equals to the net production frequency $\bar{\nu}_i$:

$$\frac{1}{n_e} \frac{\partial n_e}{\partial t} = \bar{\nu}_i = N \gamma \int_0^\infty \left(\sum_{k=\text{ionization}} \sigma_k \right) \times \epsilon F_0 d\epsilon. \quad (4.9)$$

In [26] the attachment process is also considered and it takes place in the above equation. Equation (4.5) can be written as

$$F_1 = \frac{E}{N} \frac{1}{\tilde{\sigma}_m} \frac{\partial F_0}{\partial \epsilon},$$

where

$$\tilde{\sigma}_m = \sigma_m + \frac{\bar{v}_i}{N\gamma\epsilon^{1/2}}.$$

Substituting these into Eq. (4.4), we obtain

$$-\frac{\gamma}{3} \frac{\partial}{\partial \epsilon} \left(\left(\frac{E}{N} \right)^2 \frac{\epsilon}{\tilde{\sigma}_m} \frac{\partial F_0}{\partial \epsilon} \right) = \tilde{C}_0 + \tilde{R}, \quad (4.10)$$

where

$$\begin{aligned} \tilde{C}_0 &= 2\pi\gamma^3\epsilon^{1/2} \frac{C_0}{Nn}, \\ \tilde{R} &= -\frac{\bar{v}_i}{N}\epsilon^{1/2}F_0. \end{aligned}$$

On the other hand, steady state experiments need to be considered with exponential spatial growth without time dependence. This case is more convenient to DC gas discharges. Equation (4.5) for this case is expressed as

$$F_1 = \frac{1}{\sigma_m} \left(\frac{E}{N} \frac{\partial F_0}{\partial \epsilon} + \frac{\alpha}{N} F_0 \right),$$

and Eq. (4.4)

$$-\frac{\gamma}{3} \frac{\partial}{\partial \epsilon} \left(\left(\frac{E}{N} \right)^2 \frac{\epsilon}{\tilde{\sigma}_m} \frac{\partial F_0}{\partial \epsilon} \right) = \tilde{C}_0 + \tilde{R}, \quad (4.11)$$

where

$$\begin{aligned} \tilde{R} &= \frac{\alpha}{N} \frac{\gamma}{3} \left[\frac{\epsilon}{\sigma_m} \left(2 \frac{E}{N} \frac{\partial F_0}{\partial \epsilon} + \frac{\alpha}{N} F_0 \right) + \frac{E}{N} F_0 \frac{\partial}{\partial \epsilon} \left(\frac{\epsilon}{\sigma_m} \right) \right], \\ \alpha &= \frac{1}{2D} (\mu E - \sqrt{(\mu E)^2 - 4D\bar{v}_i}) \end{aligned}$$

Here α is Townsend coefficient. Collision terms can be divided into electron - electron collision and contributions from all different collision processes is

$$\tilde{C}_0 = \sum_k \tilde{C}_{0,k} + \tilde{C}_{0,e}. \quad (4.12)$$

Electron - electron collision term is obtained after some manipulation [26] as

$$\tilde{C}_{0,e} = a \frac{n}{N} \frac{\partial}{\partial \epsilon} \left[3A_1 F_0 + 2(A_2 + \epsilon^{3/2} A_3) \frac{\partial F_0}{\partial \epsilon} \right]. \quad (4.13)$$

Description of terms in (4.13) as follows [26]:

$$\begin{aligned}
A_1 &= \int_0^\epsilon u^{1/2} F_0(u) du, \\
A_2 &= \int_0^\epsilon u^{3/2} F_0(u) du, \\
A_3 &= \int_0^\infty F_0(u) du, \\
\Lambda &= \frac{12\pi(\epsilon_0 k_B T_e)^{3/2}}{e^3 n^{1/2}}, \\
a &= \frac{e^2 \gamma}{24\pi \epsilon_0^2} \ln \Lambda, \\
k_B T_e &= \frac{2}{3} e A_2(\infty).
\end{aligned}$$

Combining these relations, the equation for EEDF can be written in a more familiar form, which is formally the stationary convection-diffusion equation:

$$\frac{d}{d\epsilon} \left(\tilde{W} F_0 - \tilde{D} \frac{dF_0}{d\epsilon} \right) = \tilde{S}, \quad (4.14)$$

where

$$\begin{aligned}
\tilde{W} &= -\gamma \epsilon^2 \sigma_\epsilon - 3a \frac{n}{N} A_1, \\
\tilde{D} &= \frac{\gamma}{3} \left(\frac{E}{N} \right)^2 \frac{\epsilon}{\tilde{\sigma}_m} + \frac{\gamma k_B T_e}{e} \epsilon^2 \sigma_\epsilon + 2a \frac{n}{N} (A_2 + \epsilon^{3/2} A_3), \\
\sigma_\epsilon &= \sum_{k=\text{elastic}} \frac{2m}{M_k} \sigma_k, \\
\tilde{S} &= \sum_{k=\text{inelastic}} \tilde{C}_0 + \tilde{R}.
\end{aligned}$$

This equation for EEDF is solved with numerical techniques described in the previous chapter. We imposed the following boundary conditions:

$$\frac{\partial f}{\partial \epsilon} = 0 \quad \text{at} \quad \epsilon = 0$$

$$f = 0 \quad \text{at} \quad \epsilon = \epsilon_{\text{final}}$$

where ϵ_{final} is the maximum energy to be considered. Discretization for inelastic terms on RHS is done in the following form [26]:

$$\int_{\epsilon_{i-1/2}}^{\epsilon_{i+1/2}} \tilde{S} d\epsilon \equiv -P_i F_{0,i} + \sum_j Q_{i,j} F_{0,j}, \quad (4.15)$$

where scattering-out and scattering-in terms are

$$P_i = \sum_{inelastic} \gamma \int_{\epsilon_{i-1/2}}^{\epsilon_{i+1/2}} \epsilon \sigma_k \exp[(\epsilon_i - \epsilon)g_i] d\epsilon,$$

$$Q_{i,j} = \sum_{inelastic} \gamma \int_{\epsilon_1}^{\epsilon_2} \epsilon \sigma_k \exp[(\epsilon_j - \epsilon)g_j] d\epsilon,$$

and $[\epsilon_1, \epsilon_2]$ interval is the overlap of j^{th} and i^{th} cells after being shifted by threshold energies u_k :

$$\epsilon_1 = \min(\max(\epsilon_{i-1/2} + u_k, \epsilon_{j-1/2}), \epsilon_{j+1/2}),$$

$$\epsilon_2 = \min(\max(\epsilon_{i+1/2} + u_k, \epsilon_{j-1/2}), \epsilon_{j+1/2}).$$

Here g_i (and also g_j) is logarithmic slope assuming F_0 distribution is piecewise exponential in P and Q integrals. They can be expressed as

$$g_i = \frac{1}{\epsilon_{i+1} - \epsilon_{i-1}} \ln \left(\frac{F_{0,i+1}}{F_{0,i-1}} \right).$$

After finding the EEDF, the transport parameters (mobility and diffusion) and the reaction rates (k_k s) are determined from the following relations [26]:

$$\mu = -\frac{\gamma}{3N} \int_0^\infty \frac{\epsilon}{\tilde{\sigma}_m} \frac{\partial F_0}{\partial \epsilon} d\epsilon, \quad (4.16)$$

$$D = \frac{\gamma}{3N} \int_0^\infty \frac{\epsilon}{\tilde{\sigma}_m} F_0 d\epsilon, \quad (4.17)$$

$$k_k = \gamma \int_0^\infty \epsilon \sigma_k F_0 d\epsilon. \quad (4.18)$$

Additionally, Townsend coefficients are determined in the case of temporal and spatial growths:

$$\alpha_k = \frac{k_k N}{\mu E} \quad (4.19)$$

and

$$\alpha_k = \frac{k_k \alpha N}{\bar{\nu}_i}. \quad (4.20)$$

4.2 Results of BE Solver

In this section, results from BE solver are demonstrated and compared with the results of BOLSIG+[28] and the data used in [5]. Calculations are done using S.G. scheme (see Section 3). However, this time Matlab's ODE solver was not

used. Since BE solver deals with a time independent equation, formation of a tridiagonal matrix with S.G. scheme and employing tridiagonal matrix algorithm (or Thomas algorithm) is preferred. In order to validate our BE solver, first, EEDF is compared with corresponding results from BOLSIG+. Subsequently, transport coefficients and reaction rate coefficients are compared with [5]. Results for Townsend coefficient α are compared with the result from the formula given in [4] with corresponding coefficients A and B (see Eq. 2.18)

Numerical tests for BE solver were carried out for argon gas at pressure $p = 3$ Torr. The reduced electric field E/N is in the range 10-10000 Td. During the calculations, only three reactions are considered which are elastic collisions ($e+Ar \rightarrow e+Ar$), direct ionization ($e+Ar \rightarrow 2e+Ar^+$), and excitation ($e+Ar \rightarrow e + Ar^*$). In [5] which is the main reference for comparisons, there are different plasma-chemical reactions included like stepwise ionization ($e+Ar^* \rightarrow 2e+Ar^+$), penning ionization ($2Ar^* \rightarrow e + Ar^+ + Ar$) and radiation ($Ar^* \rightarrow h\nu + Ar$).

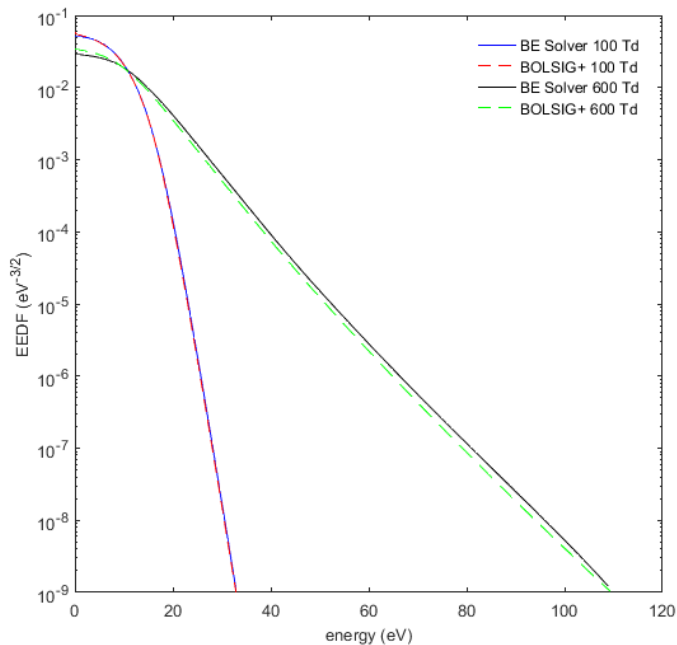


Figure 4.1: Comparison of EEDFs obtained from BE solver and from BOLSIG+[28] for two different E/N values.

Figure 4.1 shows EEDFs obtained from BE solver and from BOLSIG+[28] for two different E/N values, 100 Td and 600 Td. They are in agreement and this

validates the numerical code for BE solver module.

Figure 4.2 demonstrates EEDFs obtained from BE solver for temporal and spatial growth at $E/N = 600$ Td. Since the difference is small between the curves, both growth type can be used in discharge simulations. Comparison between EEDFs from BE solver for various reduced E -fields shows that for higher values of E/N the EEDF curve flattens as in Fig. 4.3 . In other words, for higher values of E/N , EEDF has significant contributions from high energy regions. It can be seen from Fig. 4.4, which demonstrates EEDFs obtained from BE solver for various ionization degrees n_e/N_g at reduced electric field E/N of 10 Td, that as ionization degree increases its effect on EEDF increases.

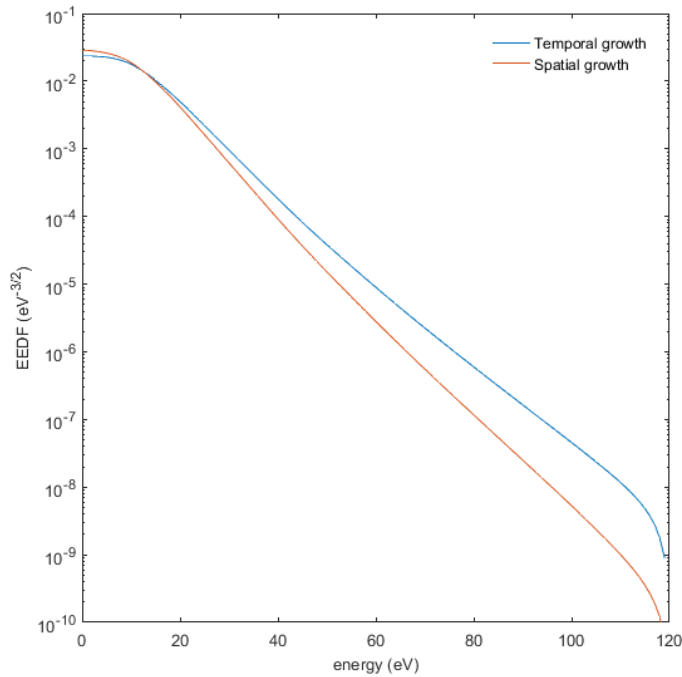


Figure 4.2: EEDFs obtained from BE solver for temporal and spatial growth at $E/N = 600$ Td.

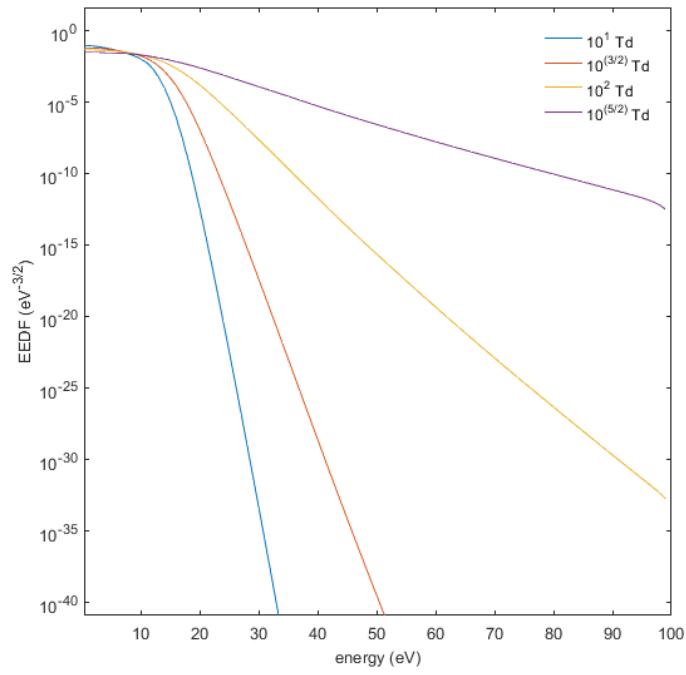


Figure 4.3: EEDFs obtained from BE solver for various reduced E -fields.

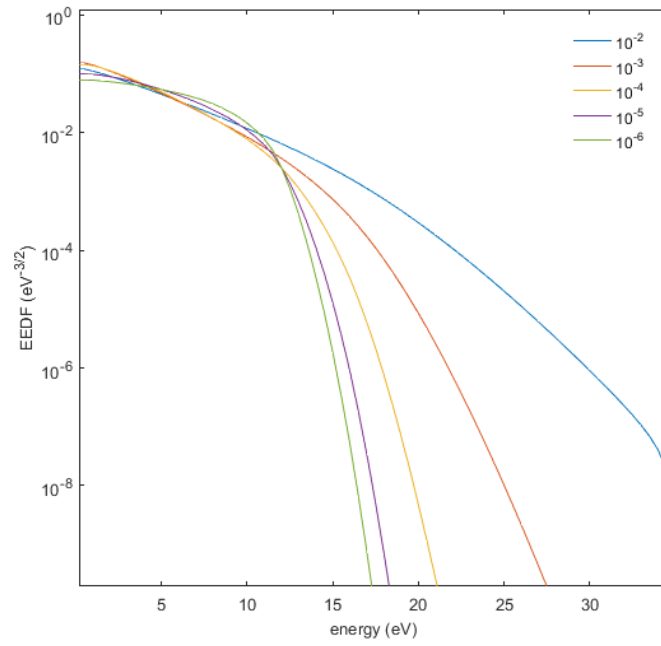


Figure 4.4: EEDFs obtained from BE solver for various ionization degrees n_e/N_g at reduced electric field E/N value 10 Td.

Fig. 4.5 compares electron mobility μ_e curves obtained from BE solver and from Ref. [5]. They are in an agreement. It should be note that plasma chemistry considered in [5] is different than ours. Reduced electric field (E/N) dependence of electron diffusion coefficients are demonstrated in Fig. 4.6. They agree sufficiently well. The small differences again can be explained by the difference in plasma chemistry. Results shown in Fig. 4.7 illustrates Townsend coefficient α obtained from BE solver and compared with formula (2.18) from Ref. [4]. As expected, they agree each other sufficiently well. Since small E -field region is not operating region for the formula (2.18) the curves deviate from one another.

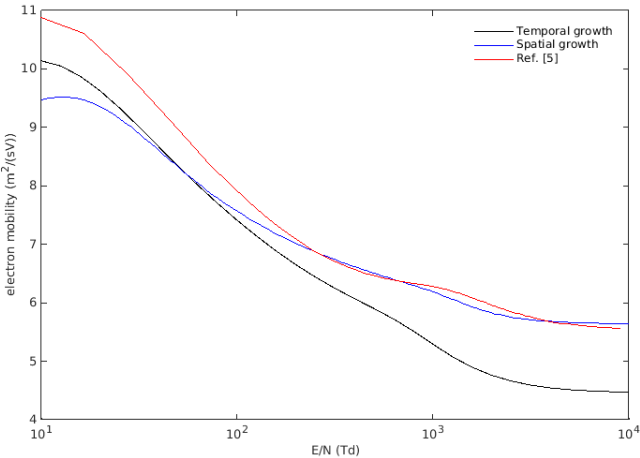


Figure 4.5: Electron mobility μ_e curves obtained from BE solver and compared with that from Ref. [5].

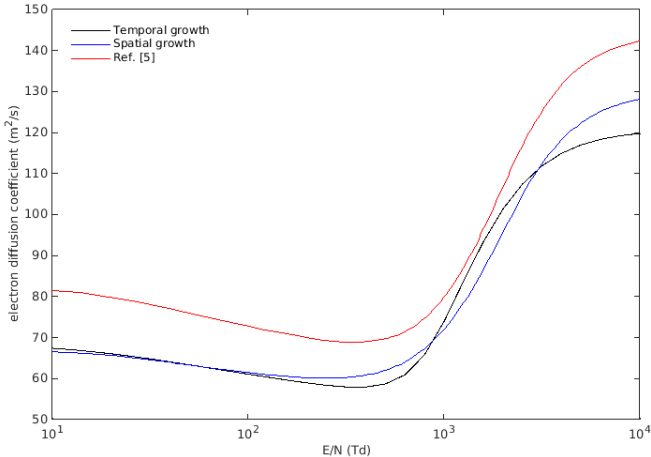


Figure 4.6: Electron diffusion coefficient D_e obtained from BE solver and compared with that from Ref. [5].

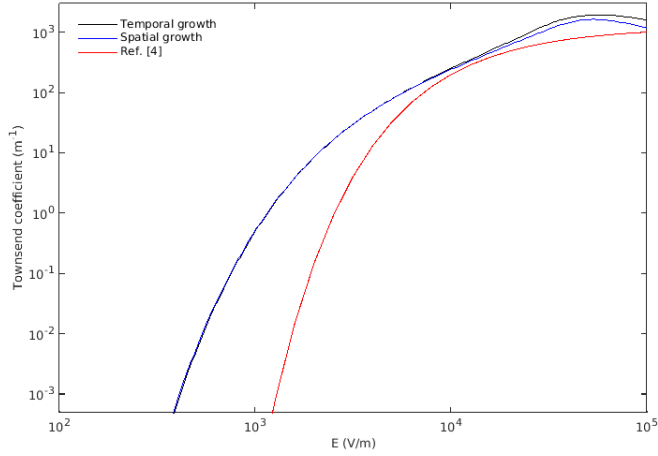


Figure 4.7: Townsend coefficient α obtained from BE solver and compared with formula from Ref. [4].

Figure 4.8 shows elastic collision frequency ν_{ie} obtained from BE solver and compared with that from Ref. [5]. The effect of different plasma chemistry explains the difference but they display the same behavior. As can be seen from Fig. 4.9 and Fig. 4.10 which compares ionization rate coefficient k_{iz} and excitation rate coefficient k_{ex} respectively, BE solver results are in acceptable agreement with the results from Ref. [5].

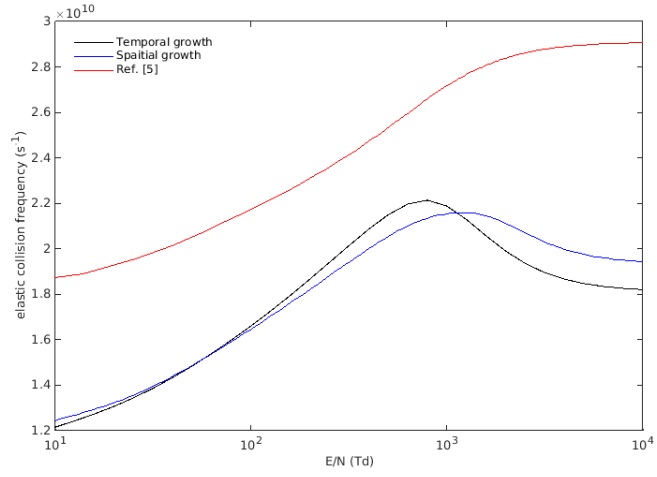


Figure 4.8: Elastic collision frequency ν_{ie} obtained from BE solver and compared with that from Ref. [5].

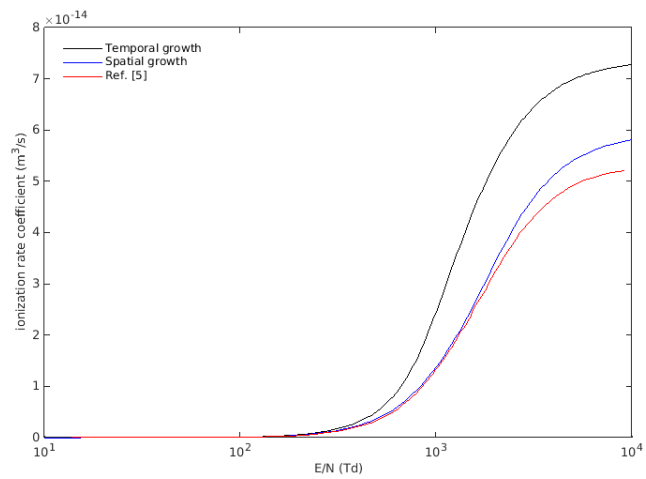


Figure 4.9: Ionization rate coefficient k_{iz} obtained from BE solver and compared with that from Ref. [5].

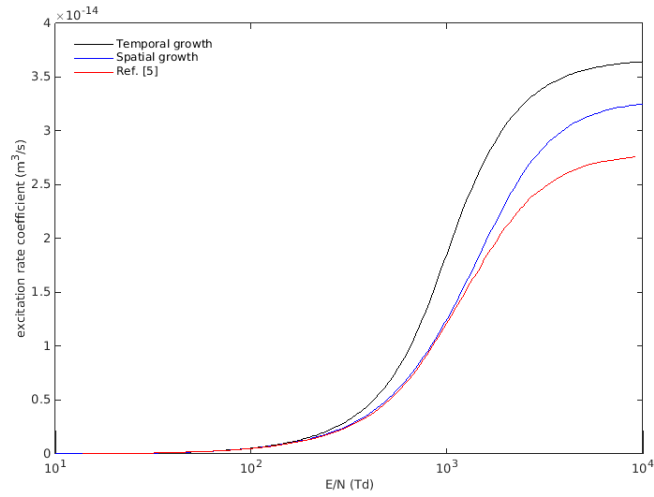


Figure 4.10: Excitation rate coefficient obtained from BE solver and compared with Ref. [5].

As can be seen from these results obtained from the BE solver module and the results computed from BOLSIG+ they are in reasonable agreement with [5] and [4].

CHAPTER 5

RESULTS OF THE FLUID MODELLING

In this chapter calculations via simple and extended models are carried out and compared with corresponding results from Refs. [5],[15] and [16]. All the calculations are performed using exponential (Scharfetter-Gummel) scheme for DC glow discharge plasma in argon gas. First, CVC curves are derived and compared with computed and experimental CVC curves from the literature. Then, the spatial distributions of basic parameters of DC glow discharge are presented and compared in abnormal, normal and subnormal regimes of the DC glow discharge. Finally, further modifications that can improve the results of the models are discussed.

5.1 CVCs and Spatial Distributions

The main difference between the extended model considered in present work and reference extended model from Ref. [5] is that in our model there is no need to include the energy equation for electrons, because in our model the local field approximation (LFA) is applied. In Ref. [26], to exclude the energy equation, usage of Townsend coefficients for ionization is recommended. Our extended model is based on this approach. Since in Ref. [5] local mean energy approximation (LMEA) is applied, source terms of the fluid equations for electrons and ions are written with reaction rate coefficients instead of Townsend coefficient. Moreover, in [5], plasma-chemical reactions include elastic collision, direct ionization excitation, stepwise ionization, penning ionization and radiation, while our extended model includes elastic collisions, direct ionization and excitation

reactions.

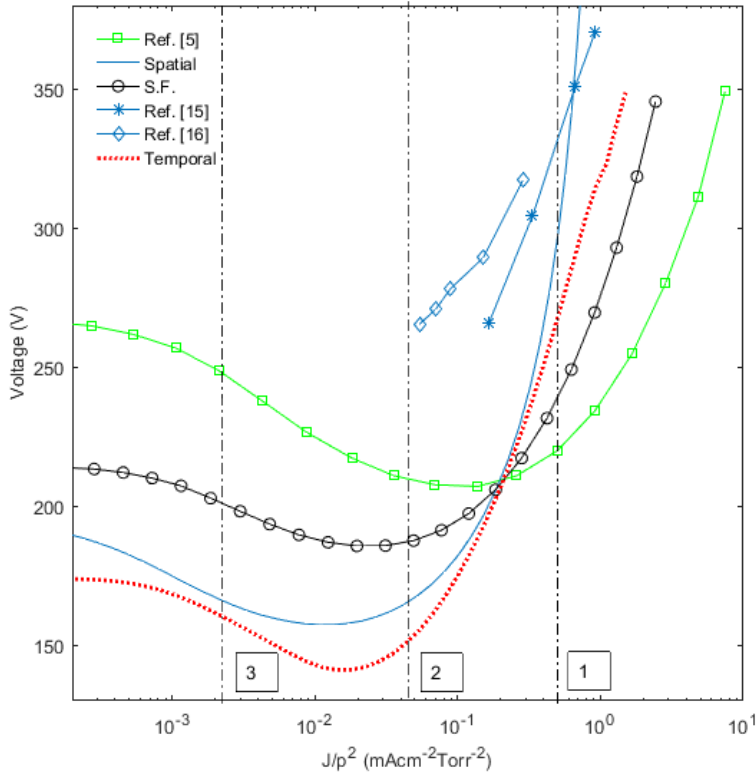


Figure 5.1: CVC curves corresponding to simple fluid, extended fluid (LFA) with spatial and temporal growth, CVC curve from extended fluid (LMEA) model [5] and two plotted experimental data from [15] and [16]. Discharge is in argon and discharge gap is 1 *cm*

Three CVC curves have been derived, one from simple fluid (S.F.) model and two from temporal and spatial growth cases within LFA and plotted in the same graph (Fig. 5.1). This figure also contains experimental CVC data [15], [16] and computed CVC from from Ref. [5]. Note that horizontal axis of CVC curves indicates reduced current densities J/p^2 where pressure is assumed to be constant $p = 3$ Torr.

The vertical axis indicates the anode voltage U_d . The CVC curves in Fig. 5.1 are in general agreement with the theoretical expectations and experimental data. The best result (nearest to experiment) is the one that obtained from the spatial growth case within LFA model. In Ref. [26] it was claimed that the temporal growth case can be used in such models. Indeed, the CVC curve for

temporal case express an acceptable pattern. The curve for simple fluid model gives relatively poorer results but still reflects a general behaviour.

Spatial distributions of plasma parameters of the simple fluid (S.F.) and extended models (LFA and LMEA) are compared in three different regimes at different the current densities. The corresponding reduced current density points are demonstrated with vertical dashed lines in Fig. 5.1. The line number shown in Fig. 5.1 indicates chosen reduced current density values that is 1 for abnormal regime, 2 for normal regime and 3 for subnormal regime.

Abnormal Regime

Figures 5.2-5.6 shows spatial distributions of plasma parameters obtained from the three different models (S.F., LFA and LMEA) in abnormal regime computed at the same current density $J = 45 \text{ A/m}^2$.

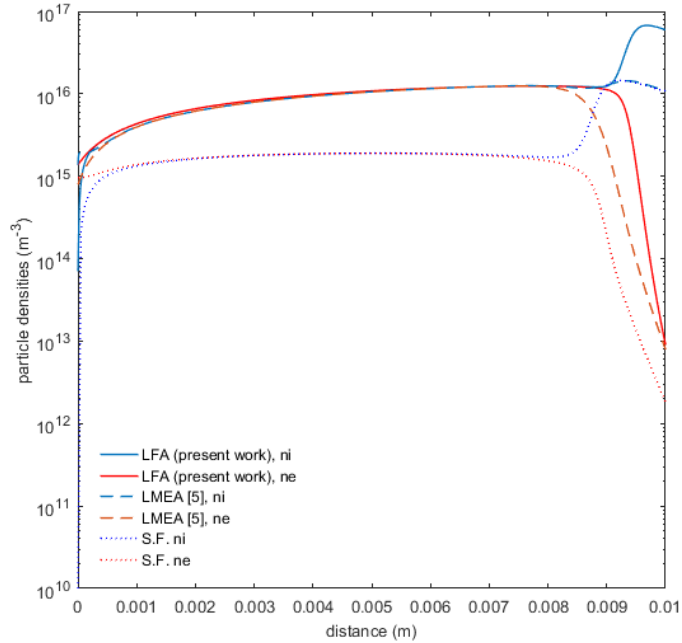


Figure 5.2: Spatial distributions of particle densities n_e and n_i obtained from the simple and extended fluid models in abnormal regime. Discharge is in argon gas, $p = 3 \text{ Torr}$, $J = 45 \text{ A/m}^2$ and discharge gap is 1 cm .

Figure 5.2 demonstrates spatial distributions of particle densities n_e and n_i ob-

tained from simple and extended fluid models in abnormal regime. As expected in abnormal regime, quasi-neutral region where $n_i \approx n_e$ occupies most of the space in the tube and cathode sheath is very narrow. As Fig. 5.3 illustrates, which is spatial distribution of ionization rates from simple and extended fluid models, ionization process occurs mainly in the narrow cathode sheath.

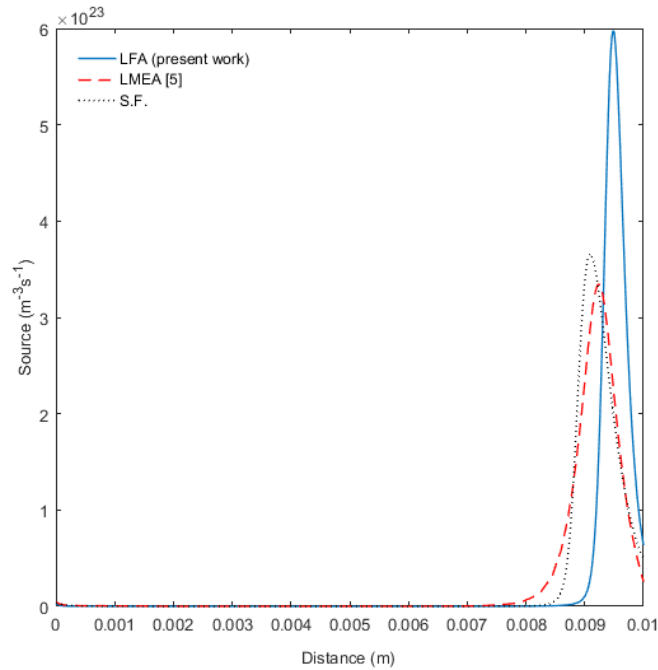


Figure 5.3: Spatial distribution of ionization rates obtained from simple and extended fluid models in abnormal regime. Conditions are the same as in Fig. 5.2.

Spatial distributions of potential Φ are illustrated in Fig. 5.4. The value at the very left indicates the anode voltage. Voltage drop in quasi-neutral region is small. However there is a rapid voltage drop in the cathode sheath. Electric field E profile is shown in Fig. 5.5. It is almost zero throughout the quasi-neutral region which can be estimated by looking the potential profile in this region. In the cathode sheath region, however, E -field increases rapidly and takes values at the order of 10^5 V/m. This explains why in the cathode sheath region the ion density is higher than the electron density. Since, electrons have higher mobilities than the ions, they moves more rapidly towards the electrodes in the presence of electric field.

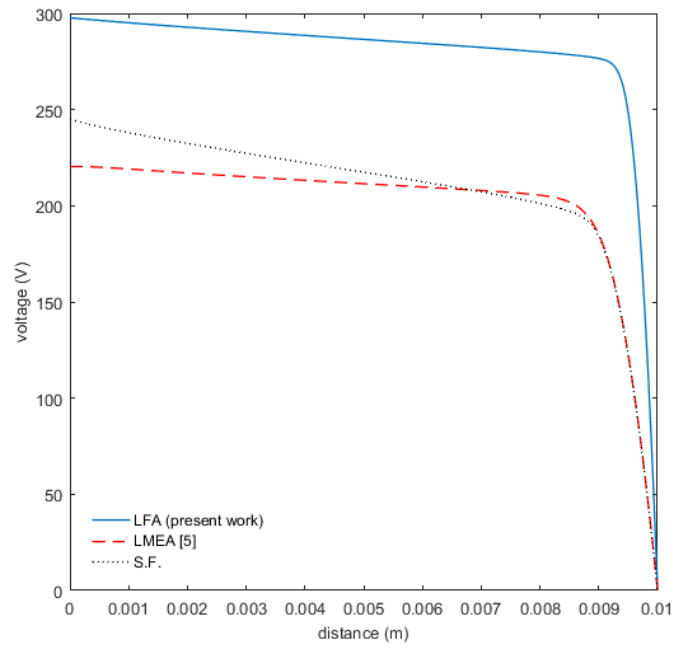


Figure 5.4: Spatial distribution of potential Φ obtained from the simple and extended fluid models in abnormal regime. Conditions are the same as in Fig. 5.2.

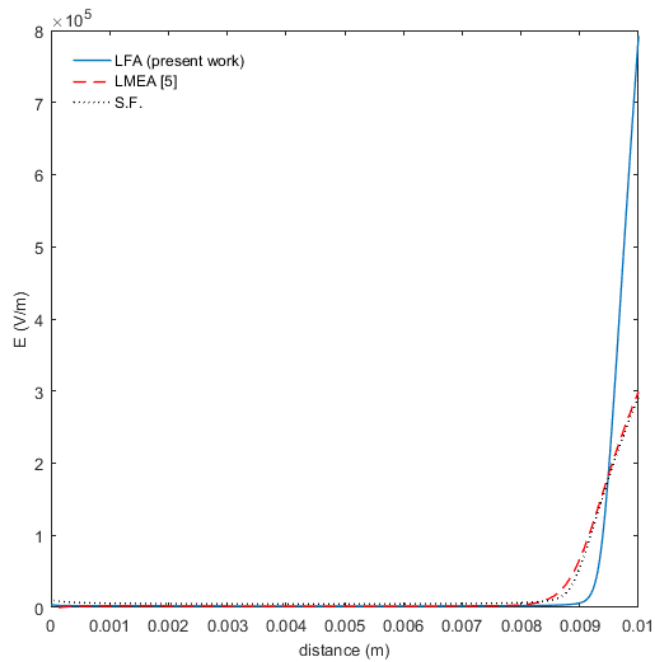


Figure 5.5: Spatial distribution of electric field E obtained from the simple and extended fluid models in abnormal regime. Conditions are the same as in Fig. 5.2.

Figure 5.6 shows spatial distribution of ion, electron and total current densities J_i , J_e and J_t , for the simple and extended fluid models in abnormal regime. Uniformity of the total current is the verification of charge conservation. There is a small region where the uniformity is distorted, which can be easily removed by grid refinement.

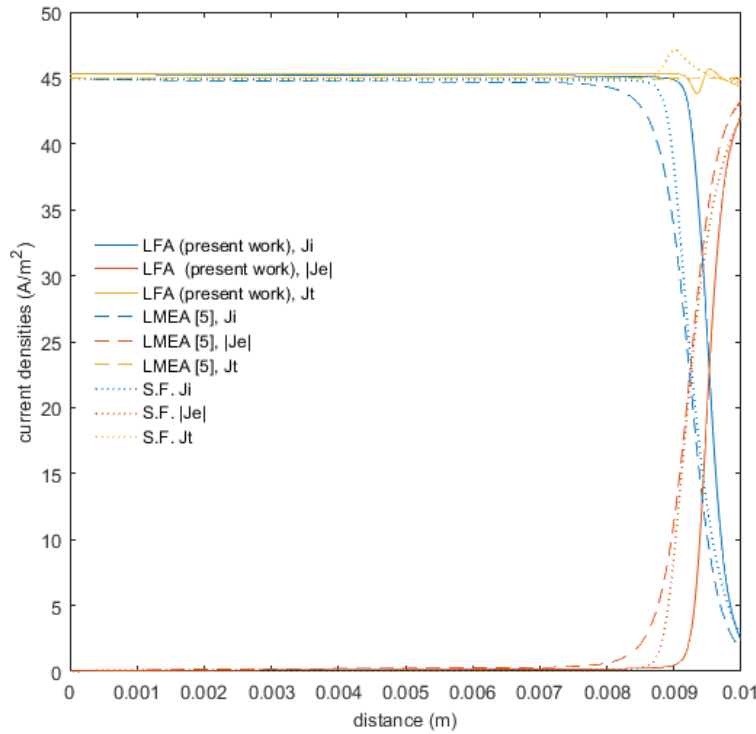


Figure 5.6: Spatial distribution of ion, electron and total current densities J_i , J_e and J_t obtained from the simple and extended fluid models in abnormal regime. Conditions are the same as in Fig. 5.2.

Normal Regime

Figures 5.7-5.11 shows spatial distribution of plasma parameters computed from the three different models (S.F., LFA and LMEA) in normal regime, at the same current density $J = 3 \text{ A/m}^2$.

In normal regime particle densities are smaller than in abnormal regime, as illustrated in Fig. 5.7, which indicates spatial distributions of particle densities n_e and n_i obtained from simple and extended fluid models. In this regime, cathode

sheath expands and quasi-neutral region gets narrower than in the abnormal regime. Spatial distribution of ionization rates from simple and extended fluid models are as in Fig. 5.8. As expected, ionization occurs in a wider space, the cathode sheath is wider than in the abnormal regime. In this region electric field E is smaller and Townsend coefficient α is smaller (see Fig. 4.7) correspondingly. Therefore we have smaller ionization rates in this regime. This also explains smaller values of densities in the normal regime. Since ionization rate decreases, the system settles down to the steady state at smaller densities.

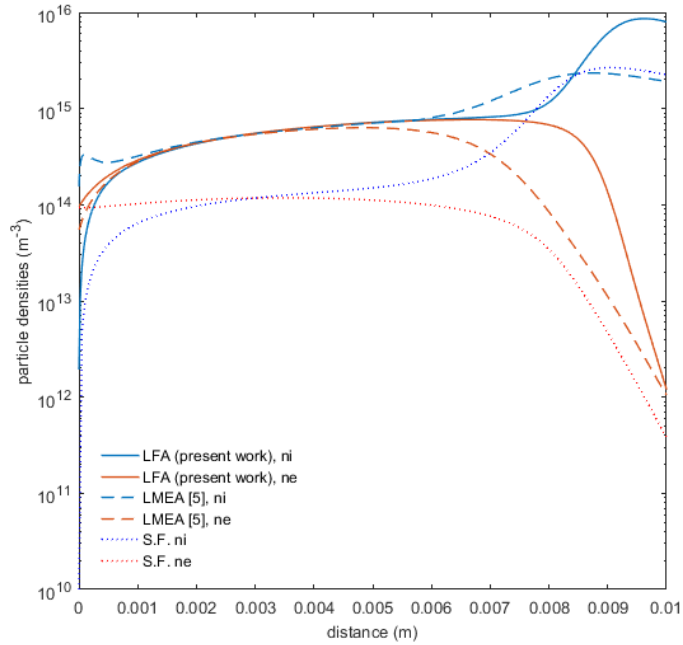


Figure 5.7: Spatial distributions of particle densities n_e and n_i obtained from the simple and extended fluid models in normal regime. Discharge is in argon gas, $p = 3$ Torr, $J = 3$ A/m² and discharge gap is 1 cm.

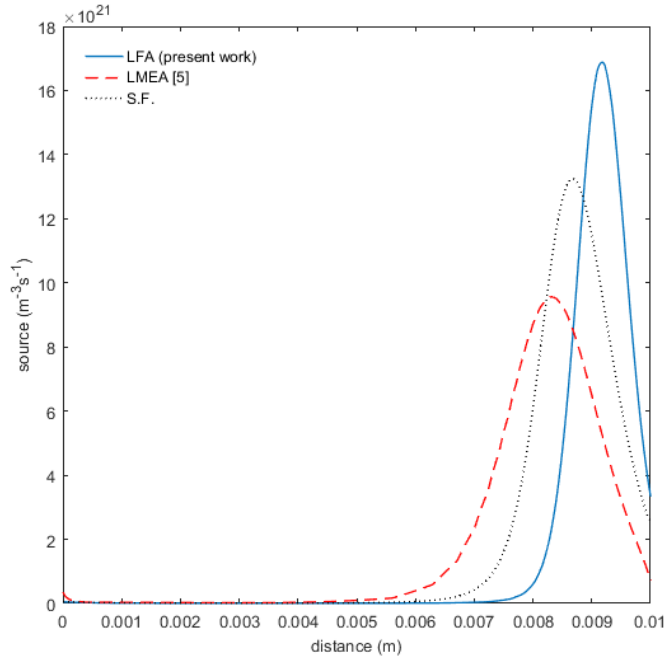


Figure 5.8: Spatial distribution of ionization rates obtained from simple and extended fluid models in normal regime. Conditions are the same as in Fig. 5.7.

In Fig. 5.9, spatial distribution of potential Φ obtained from the simple and extended fluid models is given. As expected, voltage drop in quasi-neutral region is relatively small. The voltage drop in the cathode sheath is not sharp as in the abnormal regime. The anode voltage takes smaller values compared to the other regimes as can be seen in the CVC curves in Fig. 5.1. Electric field E profiles are shown in Fig. 5.10 obtained from the simple and extended fluid models in normal regime. E -field which is mainly formed in cathode sheath is smaller than in abnormal regime.

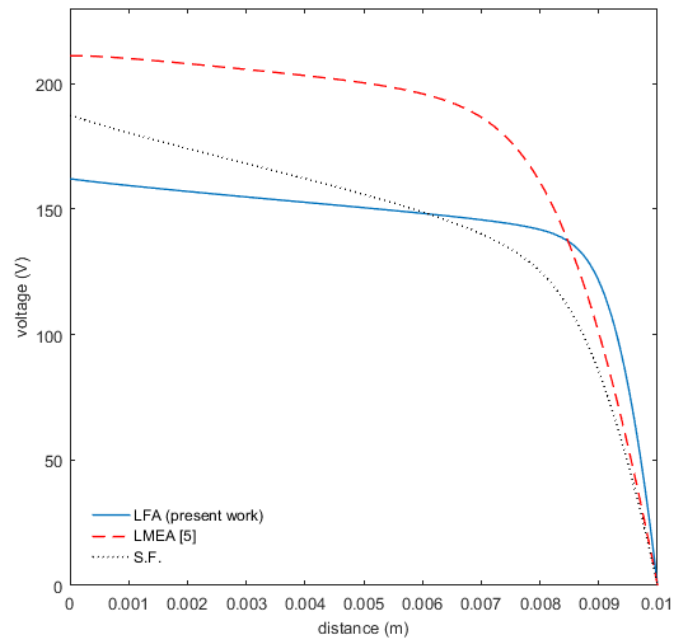


Figure 5.9: Spatial distribution of potential Φ obtained from the simple and extended fluid models in normal regime. Conditions are the same as in Fig. 5.7.

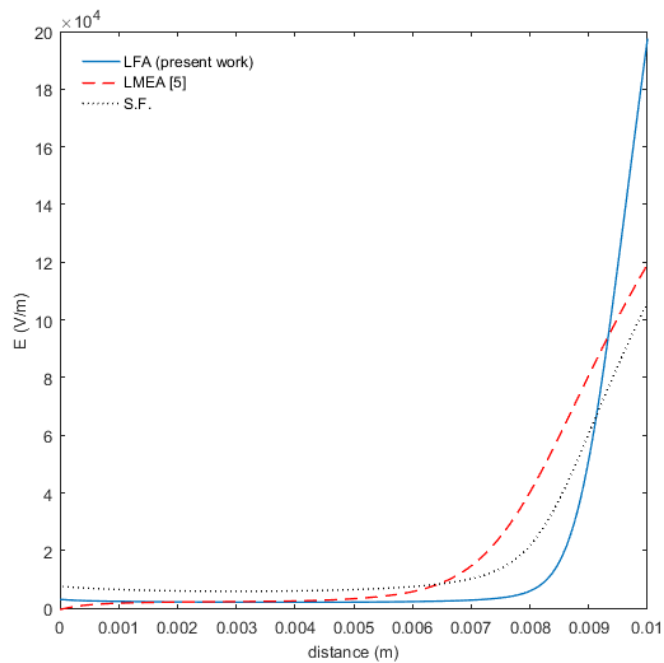


Figure 5.10: Spatial distribution of electric field E obtained from the simple and extended fluid models in normal regime. Conditions are the same as in Fig.5.7.

Figure 5.11 which illustrates spatial distributions of ion, electron and total current densities J_i , J_e and J_t , obtained from the simple and extended fluid models, verifies the charge conservation.

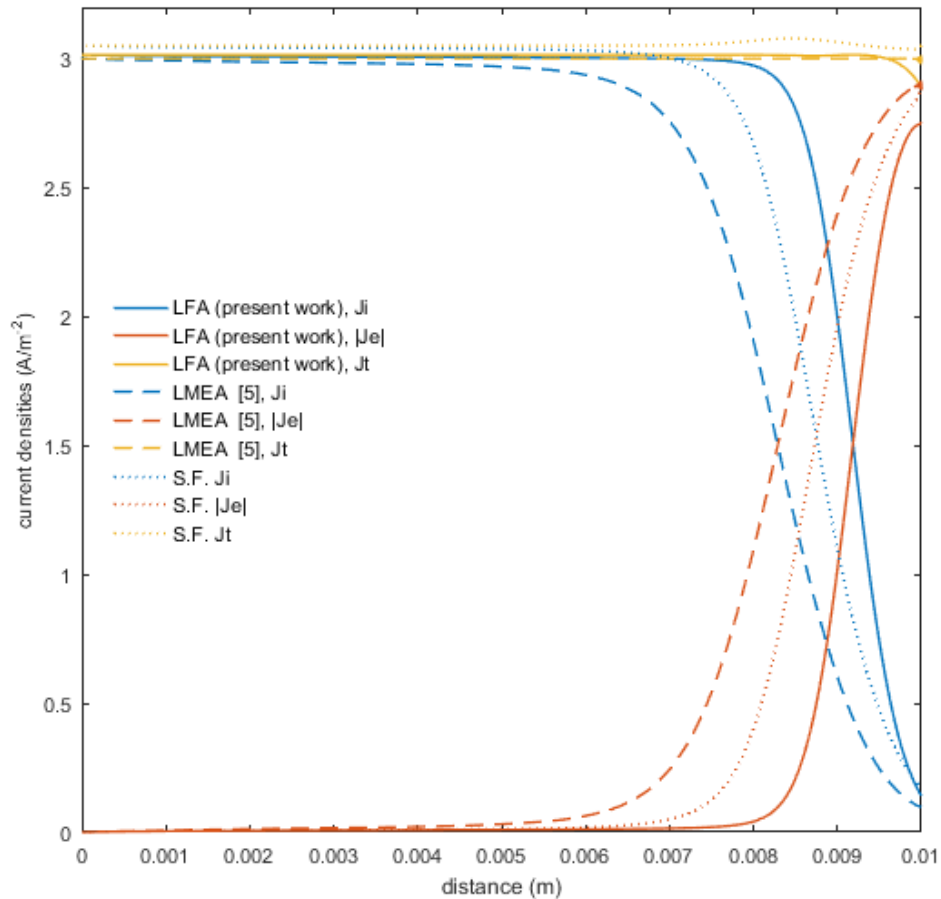


Figure 5.11: Spatial distribution of ion, electron and total current densities J_i , J_e and J_t obtained from the simple and extended fluid models in normal regime. Conditions are the same as in Fig. 5.7.

Subnormal Regime

Figs. 5.12-5.16 shows spatial distribution obtained from the plasma parameters of three different models (S.F., LFA and LMEA) in subnormal regime at the same current density $J = 0.19 \text{ A/m}^2$.

Spatial distributions of particle densities n_e and n_i obtained from simple and

extended fluid models are demonstrated in Fig. 5.12. In subnormal regime quasi-neutral region is small or even absent. Particle densities are significantly smaller than in abnormal or normal regimes. Ionization rates for the simple and extended fluid models in subnormal regime also decrease as in Fig. 5.13.

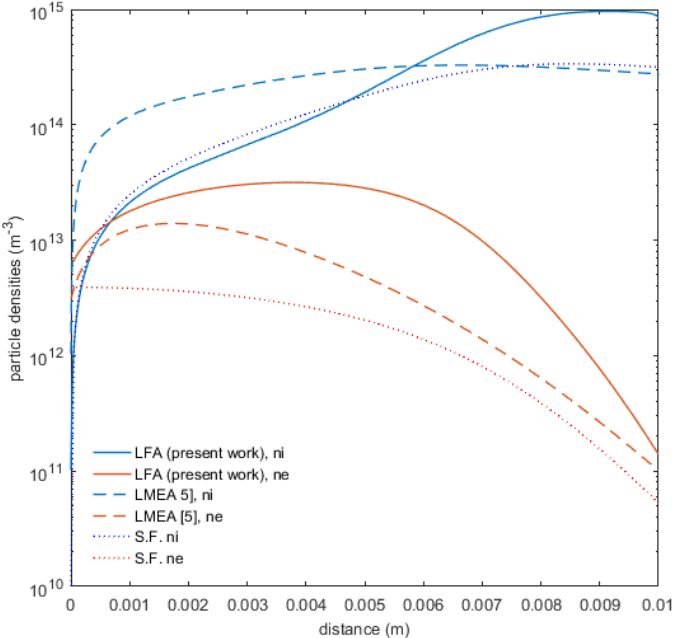


Figure 5.12: Spatial distributions of particle densities n_e and n_i obtained from the simple and extended fluid models in subnormal regime. Discharge is in argon gas, $p = 3$ Torr, $J = 0.19$ A/m² and discharge gap is 1 cm.

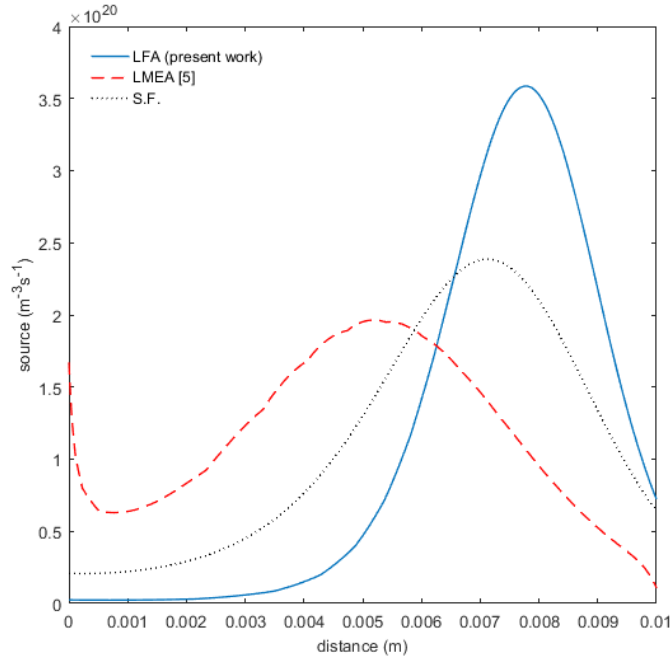


Figure 5.13: Spatial distribution of ionization rates obtained from the simple and extended fluid models in subnormal regime. Conditions are the same as in Fig. 5.12.

Figure 5.14 shows spatial distribution of potential Φ obtained from simple and extended fluid models in subnormal regime. In this case we have a smooth voltage drop across the tube because of lack of quasi-neutrality. Figure 5.15 shows spatial distribution of electric field E obtained from simple and extended fluid models in subnormal regime. In subnormal regime E -field forms almost everywhere in the tube even if it is weaker than as in abnormal and normal regimes in accordance with the potential distribution. Ion density is greater than electron density almost everywhere in the tube.

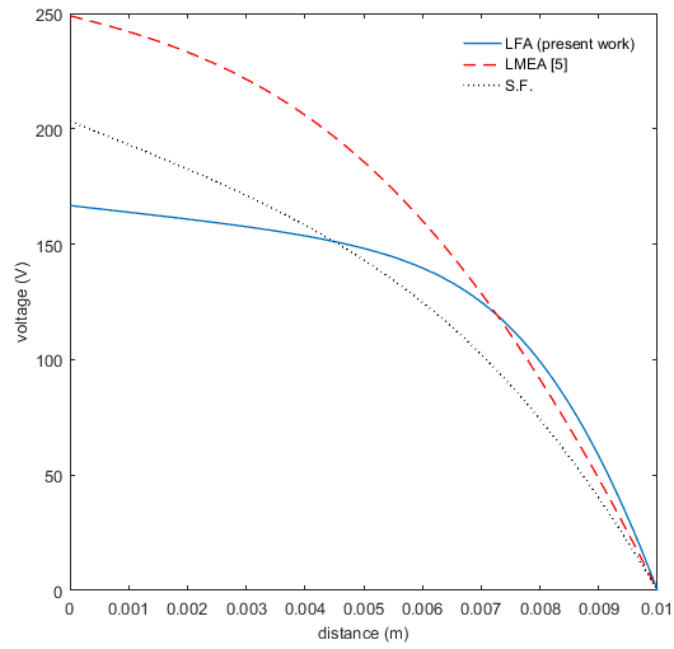


Figure 5.14: Spatial distribution of potential Φ obtained from the simple and extended fluid models in subnormal regime. Conditions are the same as in Fig. 5.12.

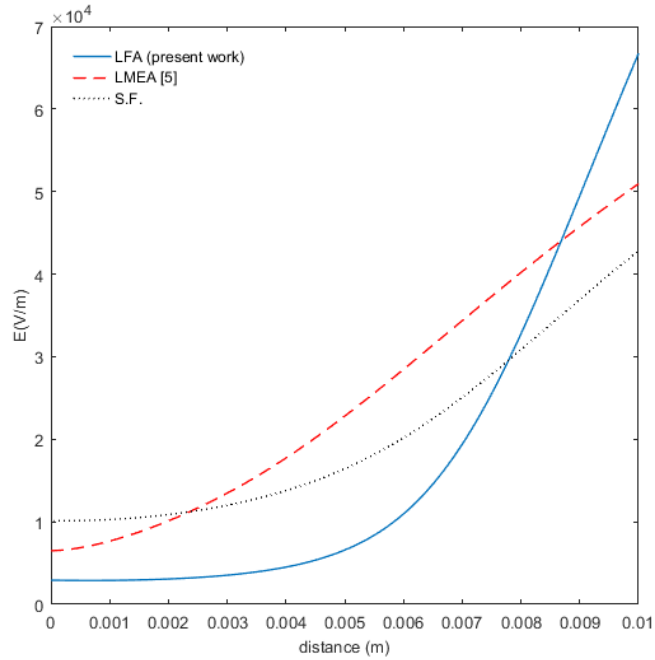


Figure 5.15: Spatial distribution of electric field E obtained from the simple and extended fluid models in subnormal regime. Conditions are the same as in Fig. 5.12.

Spatial distribution of ion, electron and total current densities J_i , J_e and J_t obtained from simple and extended fluid models are demonstrated in Fig. 5.16. We observe again charge conservation in this figure.

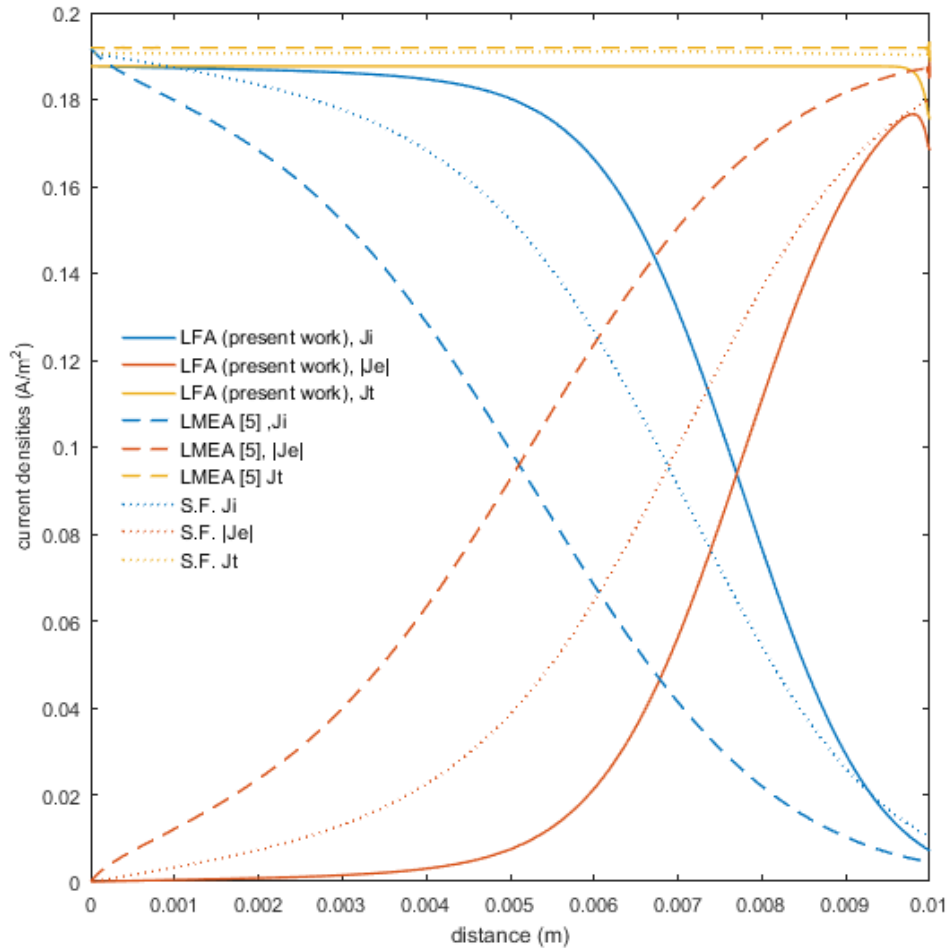


Figure 5.16: Spatial distribution of ion, electron and total current densities J_i , J_e and J_t obtained from the simple and extended fluid models in subnormal regime. Conditions are the same as in Fig. 5.12.

There are possible improvements that can be applied on extended fluid model. First modification can be done in BE solver. In Fig. 4.4 it can be observed that EEDF is different for different ionization degrees. Instead of tabulating an average ionization degree value, a 2D table can be prepared for 2D interpolation. Thus, transport coefficients and reaction rates will depend on not only the local reduced electric field E/N but also on the local value of degree of ionization.

Another suggestion to improve the BE solver module is to use adaptive ranges for EEDF and corresponding grids. As in Fig. 4.1, EEDF has higher values at the same energy for higher reduced electric fields E/N . Therefore, the position for the right end boundary for EEDF where EEDF is imposed to be zero, should be specified at higher ϵ values for higher E/N values. In other words, computational domain should be taken larger for higher E/N values. This treatment also requires an adaptive grid structure.

CHAPTER 6

CONCLUSION

In this thesis, we have studied numerically plasma properties in DC glow discharge, using two different 1D modelling approaches. These are simple fluid and extended fluid models which are based on two-fluid model of plasma with drift-diffusion approximation for particle fluxes. Numerical tests have been carried out for a DC glow discharge in argon gas with between electrode distance of 1cm , at pressure $p = 3$ Torr.

First we have developed Boltzmann equation (BE) module following the method in [26]. BE module has been validated by comparison with the results of BOL-SIG+ [28]. Then using BE solver we have derived look-up tables (LUTs) for the electron transport parameters as well as the reaction rate coefficients.

Calculations were carried out for simple fluid model with transport coefficients from [29], while for the extended fluid model, the coefficients for electrons were taken from the LUTs created from the BE solver. The MOL (Method of Lines) technique was applied to convert PDEs to ODEs. For solution of ODEs, MATLAB ode15s ODE solver was used. Discretization in spatial domain was done with finite volume method (FVM) using Scharfetter–Gummel (exponential) scheme.

We obtained CVC curves from simple fluid model and extended fluid model with local field approximation (LFA) and compared them with experimental data [15],[16] and results of extended fluid model with local mean energy approximation (LMEA) [5]. The analysis has also been done for spatial distributions of

plasma parameters in abnormal, normal and subnormal regimes of the DC glow discharge.

Comparisons showed that the extended fluid model with local field approximation (LFA) presents an agreement with experimental results in the abnormal regime. In normal regime, computed models are also in an acceptable agreement. However, in subnormal regime where the electric fields become weaker the extended fluid model with LFA presents disagreement with others. Therefore LFA approximation is not suitable for the subnormal regime. Simple fluid model demonstrates the results that are generally in an agreement with experimental data and computed results. It can be used for getting results to see general behaviour of the system.

REFERENCES

- [1] Online Etymology Dictionary. <http://www.etymonline.com/index.php?term=plasma>.
- [2] J.A. Bittencourt. *Fundamentals of Plasma Physics*. Springer, New York, 3 edition, 2004.
- [3] Casper Budtz Jorgensen. *Studies of Electrical Plasma Discharges*. PhD thesis, Aarhus University.
- [4] Yuri P. Raizer. *Gas Discharge Physics*. Springer, 1 edition, 2001.
- [5] E. Eylenceoğlu, I. Rafatov, and A. A. Kudryavtsev. Two-dimensional hybrid Monte Carlo – fluid modelling of dc glow discharges : Comparison with fluid models , reliability , and accuracy. *Phys. Plasmas*, 013509:1–9, 2015.
- [6] A. Michael Liebermann and Lichtenberg J. Allan. *Plasma Discharges and Material Processing*. John Wiley & Sons, New Jersey, 2005.
- [7] What is a gas discharge and what is used for? <https://www.uantwerpen.be/en/rg/plasmant/research/research-topics/gas-discharge-plasma/>.
- [8] J. van Dijk, G. M. W. Kroesen, and A. Bogaerts. Plasma modelling and numerical simulation. *Journal of Physics D: Applied Physics*, 42(19):190301, 2009.
- [9] Kinetic Theory. <http://web.physics.udel.edu/research/plasma-physics/kinetic-theory>.
- [10] Markus M. Becker and Detlef Loffhagen. Derivation of Moment Equations for the Theoretical Description of Electrons in Nonthermal Plasmas. *Advances in Pure Mathematics*, 03(03):343–352, 2013.
- [11] F. Iza, S. H. Lee, and J. K. Lee. *Computer modeling of low-temperature plasmas*, volume 661. 2007.
- [12] J. P. Tu, M. S. Liu, and Z. Y. Mao. High Temperature. 1648(96):43–48, 1997.
- [13] Vladimir Kolobov and Robert Arslanbekov. Deterministic Boltzmann solver for electron kinetics in plasma reactors for microelectronics applications. *Microelectronic Engineering*, 69(2-4):606–615, 2003.
- [14] Optical Society of America imagebank. <http://imagebank.osa.org/getImage.xqy?img=dTcqLmxhcmdlLGFvLTE1LTYtMTYxMC1nMDAx>.

- [15] K. Rózsa, A. Gallagher, and Z. Donkó. Excitation of ar lines in the cathode region of a dc discharge. *Phys. Rev. E*, 52:913–918, Jul 1995.
- [16] Ilija Stefanović and Zoran Lj. Petrović. Volt ampere characteristics of low current dc discharges in ar, h 2 , ch 4 and sf 6. *Japanese Journal of Applied Physics*, 36(7S):4728, 1997.
- [17] Modern Science. <http://lightningdividesthebandsofetime.blogspot.com.tr>.
- [18] S. Umran Inan and Marek Golkowski. *Principles of Plasma Physics for Enginners and Scientists*. Cambridge University Press, New York, 2011.
- [19] Francis F. Chen. *Introduction to Plasma Physics*. Springer, New York, 1 edition, 1974.
- [20] S. Surzhikov and J. Shang. Normal glow discharge in axial magnetic field. *Plasma Sources Science and Technology*, 23(5):54017, 2014.
- [21] Sergey T. Surzhikov and Joseph S. Shang. Two-component plasma model for two-dimensional glow discharge in magnetic field. *Journal of Computational Physics*, 199(2):437–464, 2004.
- [22] I. Rafatov, E. A. Bogdanov, and A. A. Kudryavtsev. On the accuracy and reliability of different fluid models of the direct current glow discharge. *Physics of Plasmas*, 19(3):1–12, 2012.
- [23] William Schieser and Graham W. Griffiths. *A Compendium of Partial Differential Equation Models*. Cambridge University Press, New York, 2009.
- [24] Suhas V. Patankar. *Numerical Heat Transfer and Fluid Flow*. McGraw-Hill.
- [25] D. L. Scharfetter and H. K. Gummel. Large-signal analysis of a silicon read diode oscillator. *IEEE Transactions on Electron Devices*, 16(1):64–77, Jan 1969.
- [26] G. J. M. Hagelaar and L. C. Pitchford. Solving the Boltzmann equation to obtain electron transport coefficients and rate coefficients for fluid models. *Plasma Sources Sci. Technol.*, 14(14):722–733, 2005.
- [27] L. C. Pitchford, S. V. O’Neil, and J. R. Rumble. Extended boltzmann analysis of electron swarm experiments. *Phys. Rev. A*, 23:294–304, Jan 1981.
- [28] BOLSIG. <https://www.bolsig.laplace.univ-tlse.fr/>.
- [29] I. R. Rafatov, D. Akbar, and S. Bilikmen. Modelling of non-uniform DC driven glow discharge in argon gas. *Physics Letters, Section A: General, Atomic and Solid State Physics*, 367(1-2):114–119, 2007.